



Virtual screening of quinoline derived library for SARS-COV-2 targeting viral entry and replication

Anju Anju^{a,b} , Shubhra Chaturvedi^b , Vishakha Chaudhary^{a,b} , Pradeep Pant^c , Firasat , Hussain^a and Anil Kumar Mishra^b

^aDepartment of Chemistry, University of Delhi, Delhi, India; ^bDivision of Cyclotron and Radiopharmaceutical Sciences, Institute of Nuclear Medicine and Allied Sciences, Defence Research and Development Organization Brig, Delhi, India; ^cDepartment of Chemistry, Indian Institute of Technology, New Delhi, India

Communicated by Ramaswamy H. Sarma

ABSTRACT

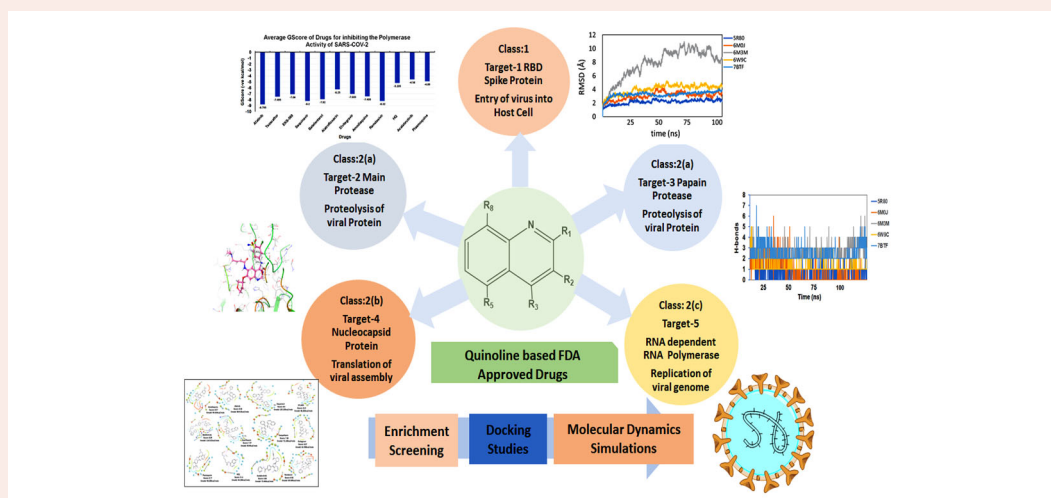
The COVID-19 pandemic infection has claimed many lives and added to the social, economic, and psychological distress. The contagious disease has quickly spread to almost 218 countries and territories following the regional outbreak in China. As the number of infected populations increases exponentially, there is a pressing demand for anti-COVID drugs and vaccines. Virtual screening provides possible leads while extensively cutting down the time and resources required for ab-initio drug design. We report structure-based virtual screening of a hundred plus library of quinoline drugs with established antiviral, antimalarial, antibiotic or kinase inhibitor activity. In this study, targets having a role in viral entry, viral assembly, and viral replication have been selected. The targets include: 1) RBD of receptor-binding domain spike protein S 2) M^{PRO} Chymotrypsin main protease 3) P^{PRO} Papain protease 4) RNA binding domain of Nucleocapsid Protein, and 5) RNA Dependent RNA polymerase from SARS-COV-2. An in-depth analysis of the interactions and G-score compared to the controls like hydroxyquinoline and remdesivir has been presented. The salient results are (1) higher scoring of antivirals as potential drugs (2) potential of afatinib by scoring as better inhibitor, and (3) biological explanation of the potency of afatinib. Further MD simulations and MM-PBSA calculations showed that afatinib works best to interfere with the the activity of RNA dependent RNA polymerase of SARS-COV-2, thereby inhibiting replication process of single stranded RNA virus.

ARTICLE HISTORY

Received 14 September 2020
Accepted 31 March 2021

KEYWORDS

SARS-COV-2; RNA dependent RNA polymerase; Bruton Tyrosine kinase inhibitors; quinoline based FDA approved Drugs



Abbreviations: COVID-19: Corona Virus Disease-2019; SARS-COV-2: Severe Acute Respiratory Syndrome-2; FDA: Food and Drug Administration; PK: Pharmacokinetic Properties; HCQ: Hydroxychloroquine; RdRp: RNA Dependent RNA Polymerase; BTK: Bruton Tyrosine Kinase; 2D: Two Dimensional

1. Introduction

The pandemic outbreak of novel severe acute respiratory syndrome 2 or COVID-19 has claimed many lives and added to the social, economic, and psychological distress (Huang et al., 2020). Initially, the outbreak was local in Wuhan, China. With time the virus spread exponentially across borders through human contact. Considering the grave gravity, the World Health Organization (WHO) declared COVID-19 pandemic, a public health emergency of international concern (Law, 2020).

The continuously growing numbers of infections and mortality worldwide have called for a prompt therapeutic solution against COVID-19. Currently, no drugs or vaccines can specifically target the proteins in the corona virus to prevent diseases; hence the discovery of drugs or vaccines may be a milestone for all researchers. Based on clinical experiences while treating moderate to severe cases, three drugs-hydroxyquinoline, (Rothan & Byrareddy, 2020) remdesivir (Ko et al., 2020) and, lopinavir/ritonavir (Chu et al., 2004) have emerged with varied and contentious potential. Vaccine development is under progress. However, the chances of a breakthrough are bleak in the immediate future.

The pressing and expeditious demand for an effective therapeutic clubbed with limited biochemical knowledge, and complex-tedious-resource intensive drug designing have compelled researchers to switch to virtual screening for drug molecules. Drug repurposing through virtual screening is an innovative approach in the current time to quickly arrive at the promising scaffold (Kiplin Guy et al., 2020; Shah et al., 2020).

Taking leads from the limited and not-so successful clinical experiences, we hypothesize that virtual screening of drugs similar to hydroxyquinoline (HQ), remdesivir, and lopinavir/ritonavir might provide potential scaffolds. The three drugs target different pathways in effective scenarios: hydroxyquinoline acts as inhibitors during the entry of viral particles (Liu et al., 2020), remdesivir interfere with RNA replication (Yin et al., 2020), lopinavir/ritonavir (Cao et al., 2020) inhibits the activity of the virus by interfering with essential protein necessary for their life cycle. Among them, our interest focuses on hydroxyquinoline derived molecules because: (1) It is a proven antimalarial drug and antiviral, primarily acting as entry inhibitor and in some cases as endosomal pH modulator interfering with viral release, (2) It is an attractive pharmacophore for many protease inhibitors like the inhibitors for Fibroblast activated protein (FAP: Ramser et al., 2009), Bacillus thuringiensis serotype Kurstaki(BTK) proteases: (Barnard et al., 2014), Platelet-Derived Growth Factor (PDGFR), and as ALK5 inhibitors for TGF- β RI Kinase, and (3) It also acts as an immunomodulator. Thus, the heterocycle compound quinoline and its derivatives have found applications as an anticancer, anti(myco)bacterial, antiviral, anticonvulsant, anti-inflammatory, and cardiovascular activity regulator (Marella et al., 2013).

A detailed insight into quinoline's mechanism as an anti-COVID reflects three potential targetclasses: Class 1. As an inhibitor during viral entry, Class 2. As an inhibitor for transmembrane proteases, and Class 3. As a modulator of the

immune response (Alexpandi et al., 2020). The first two target classes are primarily related to coronavirus, whereas the third class refers to the host.

The coronavirus entry into the host cell relies on the interaction of its spike glycoprotein with the Angiotensin receptor (ACE-2) of the host (human) (Shang et al., 2020). This entry mechanism is nearly universal for other members of the betacoronavirus of the coronaviridae family. The attachment to the host cells occurs through the S1 subunit of the beta-coronavirus spike proteins, marking the viral fusion (H. Chakraborty et al., 2020). Quinoline derivatives have been reported to be an antagonist for ACE2 receptors. Figure 1 summarizes some potent antagonists for the ACE2 receptor.

The ACE2 receptor facilitates the entry of the viral particles through endocytosis and allows the transfer of a single stranded RNA strand into the host cell. Proteases also mediate the entire process at different steps. Main Protease is a cysteine protease that processes itself and then cleaves into several non-structural viral proteins having roles in viral replication. Thus, the protease has been suggested as one of the most facile and pragmatic target for drug repurposing owing to its role in the viral cycle and the ease of its biochemical assays (Dai et al., 2020).

Besides the above two targets that focus on viral particles, the host immune response can help prevent the replication and infection of the virus. However, an overactive immune system can cause a cytokine storm (C. Chakraborty & Bhattacharjya, 2020) leading to life-threatening conditions. An anti-COVID agent that can avoid the overactivation of human cells and modulates the immune response can be of therapeutic utility.

Hypothesizing that quinoline derivatives can emerge as a potent anti-COVID agent, targeting either of the above targets individually or in combination, we have screened an extensive library of hundred plus FDA approved quinoline based drugs using structure-based methods. Our focus has been to target the coronavirus, and hence the first two classes of targets have been considered. Among the class 1, we selected Receptor binding Domain of Spike protein of SARS-COV-2 (PDB ID 6M0J: Target 1), and among class 2 targets we have chosen: (a) Replicase polyprotein through Main Protease Mpro of SARS-COV-2 (PDB ID 5R80: Target 2) and Papain like protease (PDB ID 6W9C: Target 3) (b) Viral assembly through N-terminal RNA binding domain of Nucleocapsid protein of SARS-COV-2 (PDB ID 6M3M: Target 4), and (c) Viral RNA synthesis by targeting RNA Dependent RNA Polymerase (PDB ID 7BTF: Target 5)

2. Methods

2.1. Drugs Screened for analysing repurposing potential

One hundredthirty-onequinoline based different category of drugs that are FDA approved as antimalarial, antiviral, inhibitors of BTK and PDGFR, antibiotics and respiratory specific-drugs were selected for structure-based screening. Appropriate controls viz., hydroxychloroquine and the non-quinoline drugs- remdesivir and galidesivir were chosen to compare the interactions. Molecular modelling Schrödinger

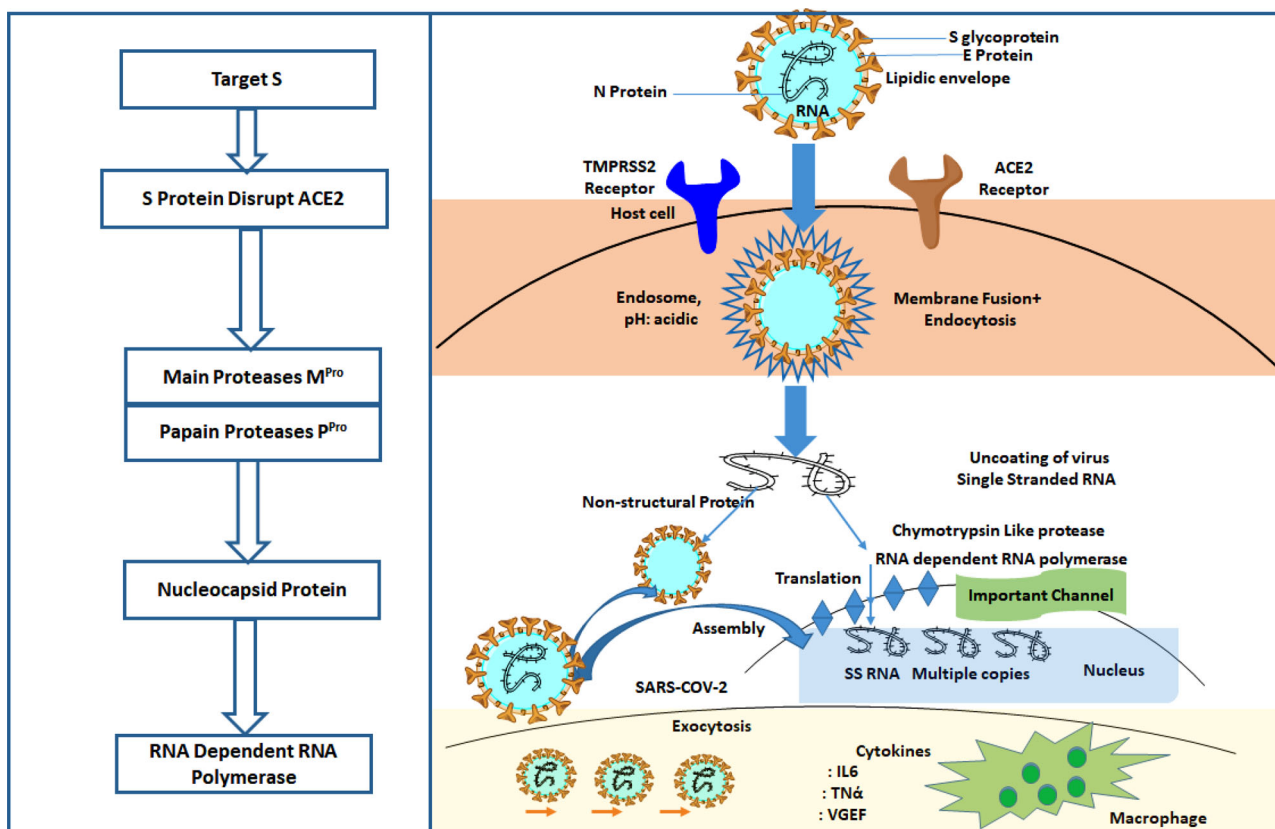


Figure 1. Showing antagonist for inhibiting the activity of SARS-COV-2 at Different stages and mechanism of SARS-COV-2 from entry into the host cell to generation of new viral species.

Software (v 2020) and Maestro 11.1 platform have been used for computational studies.

2.2. Targets selected to identify anti-COVID drug

Five targets were chosen for the study: (1) Receptor binding domain of SARS-COV-2 interacting with human ACE2 receptor (PDB ID: 6M0J) (2) chymotrypsin-like main protease of the virus M^{Pro} or 3CL Pro , (M^{Pro} , PDB ID: 5R80) (3) Papain-like Protease from SARS-COV-2PL Pro (PDB ID: 6W9C), (4) N-terminal RNA binding domain of Nucleocapsid protein of SARS-COV-2 (PDB ID: 6M3M), and (5) RNA dependent RNA Polymerase from SARS-COV-2 (PDB ID: 7BTF). Also, two additional PDBs (6LU7, 6WTT) for the target Main Protease were chosen that are co-crystallized structures with different inhibitors. The coordinates and detailed sequence information was obtained from RCSB Protein Data Bank (www.rcsb.org). The drugs were drawn using the Marvin Sketch tool as Mol2 format and imported in the software. After the ligand preparation using LigPrep v2.9 (OPLS3 force field, pH 7.0 \pm 2.0) and protein preparation using Protein Preparation Wizard followed by binding site identification using SiteMap. The grid was generated with the box-dimensions (a) 120*120*120 for 6M0J against amino acids residue within the active site having Tyr495, Tyr505, Gly496, Asn487, and Gly502 (b) 80*80*80 for 6W9C within the active site having Asp103, Gly164, and Gly270, (c) 88*88*88 for 7BTF within the active site having Asp760 and Asp761, and (d) 112*112*112 for 6M3M including residues Ala51, Tyr112, and Tyr124. For the main of

protease of SARS-COV-2, grid was generated against bound co-crystallized ligand N3 inhibitor with box dimension 72*72*72. After generation of grid docking of energy minimized ligands was performed using Extra Precision mode in Glide module.

For identification of possible receptor-ligand interaction analysis, more than five poses per ligand were selected, and docking parameters were computed using XP-visualizer. The drug interactions with the target, GScores, docking scores, and Glide EModel were thoroughly analysed to get the best interaction pose of ligand (drug) with the receptor. For all targets, appropriate controls were selected. Hydroxychloroquine serves as a control for Target S protein and M^{Pro} . Since galidesivir is screened as a potent drug for targeting RdRp polymerase, we used it as its control (Elfiky, 2020).

2.3. In silico ADME analysis

The pharmacokinetic (PK) properties of quinoline-based library viz., absorption, distribution, metabolism, excretion, and toxicity (ADMET) were calculated using the BioLuminate module of the Schrödinger Molecular Modelling Software (M/s Schrödinger, LLC, New York, NY, v. 2020).

2.4. Enrichment studies

Enrichment studies have been performed to assess the enrichment of active compounds in a screening process that

Table 1. GScore of top-ranking drugs for different category of targets 1) 6M0J 2)5R80 3) 6W9C 4) 6M3M 5) 7BTF.

Target 1 6M0J	Target 2 5R80	Target 3 6W9C	Target 4 6M3M	Target 5 7BTF
-10.8	-9.04	-8.57	-8.51	-8.97
CP609754	Afatinib	Amodiaquine	Primaquine	EKB-569
-9.72	-8.77	-8.53	-8.50	-7.81
Afatinib	Tezacaftor	Afatinib	Amodiaquine	Campothecin
-9.6	-8.48	-8.4	-7.61	-7.53
Saquinavir	EKB-569	Saquinavir	Saquinavir	Amodiaquine
-9.52	-8.00	-8.15	-7.57	-7.10
Acalabrutinib	Saquinavir	SYL1655	Elvitegravir	Primaquine
-9.41	-7.75	-8.09	-7.29	-7.04
Rilapladib	Batefenterol	Batefenterol	Imiquimod	Dequalinium
-9.02	-7.48	-7.57	-7.26	-7.04
Plasmoquine	Alatrofloxacin	Quarflorin	Afatinib	Elvitegravir
-7.4	-7.4	-7.68	-7.23	-6.7
Elvitegravir	Elvitegravir	Campothecin	Pamaquine	Imiquimod
-6.91	-6.3	-6.67	-5.15	-6.4
Amodiaquine	Amodiaquine	Elvitegravir	Acalabrutinib	Saquinavir
-6.93				
SYL1683				
-6.75	-8.02	-8.42	-6.85	-8.4
Remdesivir	Remdesivir	Remdesivir	Remdesivir	Remdesivir
				-5.37
				Galidesivir
-6.05	-5.3	-5.11	-4.99	-6.1
HQ	HQ	HQ	HQ	HQ
-4.9	-4.32	-5.77	-3.58	-5.9
EKB-569	Acalabrutinib	Plasmoquine	EKB-569	Afatinib
	-4.01	-4.84	-2.63	-5.4
	Plasmoquine	Acalabrutinib	Plasmoquine	Acalabrutinib

includes a set of actives and a set of decoys (1000 decoys). The screening can be done with any program: Glide, Shape Screening, Phase. We used Glide program (docking tool) for the screening process. The active ligands input for the panel was taken from the output from the screening program having highest GScore with each therapeutic targets of SARS-COV-2 and, set of decoys were used from Schrodinger Maestro 11.0.

2.5. Molecular Dynamics simulation

Molecular dynamics simulations have been used extensively to explore the biological processes and ligand interactions in recent years (Dror et al., 2012; Duan et al., 2019; Hollingsworth & Dror, 2018; Santhanam et al., 2019). As through docking we have screened that afatinib is the best drug among all quinoline based drugs to target proteases of SARS-COV-2. Therefore, MD simulations have been performed with Afatinib drugs with all five therapeutics targets of SARS-COV-2. We performed all-atom explicit solvent MD simulations on the docked protein-afatinib (6M0J-afatinib, 5R80-afatinib, 6W9C-afatinib, 7BTF-RdRp, 6M3M-Nprotein) complex to evaluate the binding of the afatinib at the active site of the protein with respect to the simulations run length using AMBER software (Yang et al., 2016). The geometry of the ligands was optimized, and the bond, angle, dihedral, and partial charges [RESP] were generated using HF/6-31G* in Gaussian09 (Vanqulele et al., 2011) All the ligand parameters were saved in an AMBER compatible library file for each ligand considered for the study. All the complexes were immersed in a cubic water box (TIP3P water molecules) with counterions to ensure the overall electroneutrality of

the systems. The protein counterparts were simulated with modified ff99SB force field (Maier et al., 2015), and the parameters for the counterions were taken from the literature (Joung & Cheatham, 2008).

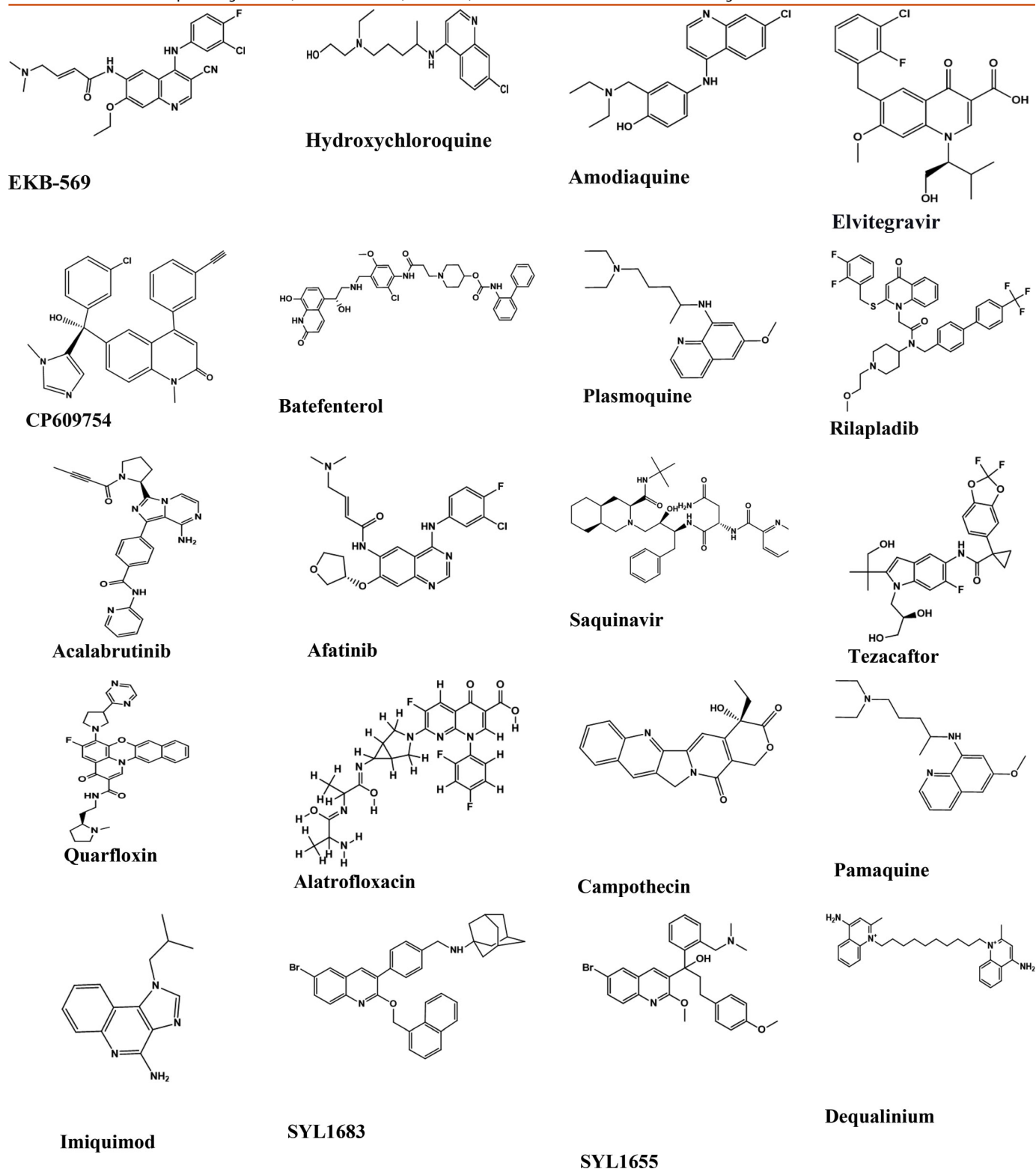
We used Particle Mesh Ewald treatment (Cheatham et al., 1995) (for long-range electrostatics) with periodic boundary conditions for performing the simulations. All the systems underwent minimization to remove close contact in the systems, if any, followed by heating (50 ps, NVT) and equilibrating (5 ns). Finally, 100 ns long MD simulations were performed. For analysis, the Cpptraj code (Roe & Cheatham, 2013) was used for computing RMSD fluctuations, structure clustering, and the number of hydrogen bonds between ligand and protein molecules.

2.6. MM-PBSA calculation

LigPlot + software (Laskowski & Swindells, 2011) was used to sketch the interactions of the afatinib with protein. Molecular Mechanic/Poisson Boltzmann Surface Area (MM-PBSA) (Onufriev et al., 2000) calculations were performed to evaluate the binding proclivity of the ligand to the protein. The binding free energy gives information about different kind of interactions (potential energy and polar and non-polar solvation energy) and computed by using the following equation: (Bhardwaj et al., 2020)

$$\Delta G_{\text{binding}} = G_{\text{complex}} - (G_{\text{receptor}} + G_{\text{ligand}})$$

where $\Delta G_{\text{binding}}$ refers to change in energy after the formation of afatinib- ligand complex and G_{receptor} is energy of free receptor without afatinib and G_{ligand} is the energy of afatinib + in unbound form.

Table 2. Illustrations of top-ranking antiviral, antimalarial and, antibiotic, kinase inhibitor and anti-asthmatic Drugs.

3. Results and discussion

3.1. Docking and analysis

Quinoline pharmacophore is an important moiety according to the biological point of view. Its derivatives have been used in many fields for the progression of Alzheimer's

diseases (Sureshkumar et al., 2020) as an antimalarial drug target serine protease as an anticancer agent, and as an antimicrobial and antifungal agent (Marella et al., 2013; Desai et al., 2017). Hence in present work, we have reported in silico studies of quinoline-based, FDA-approved drugs for docking studies with crystal structures of SARS-COV-2. We

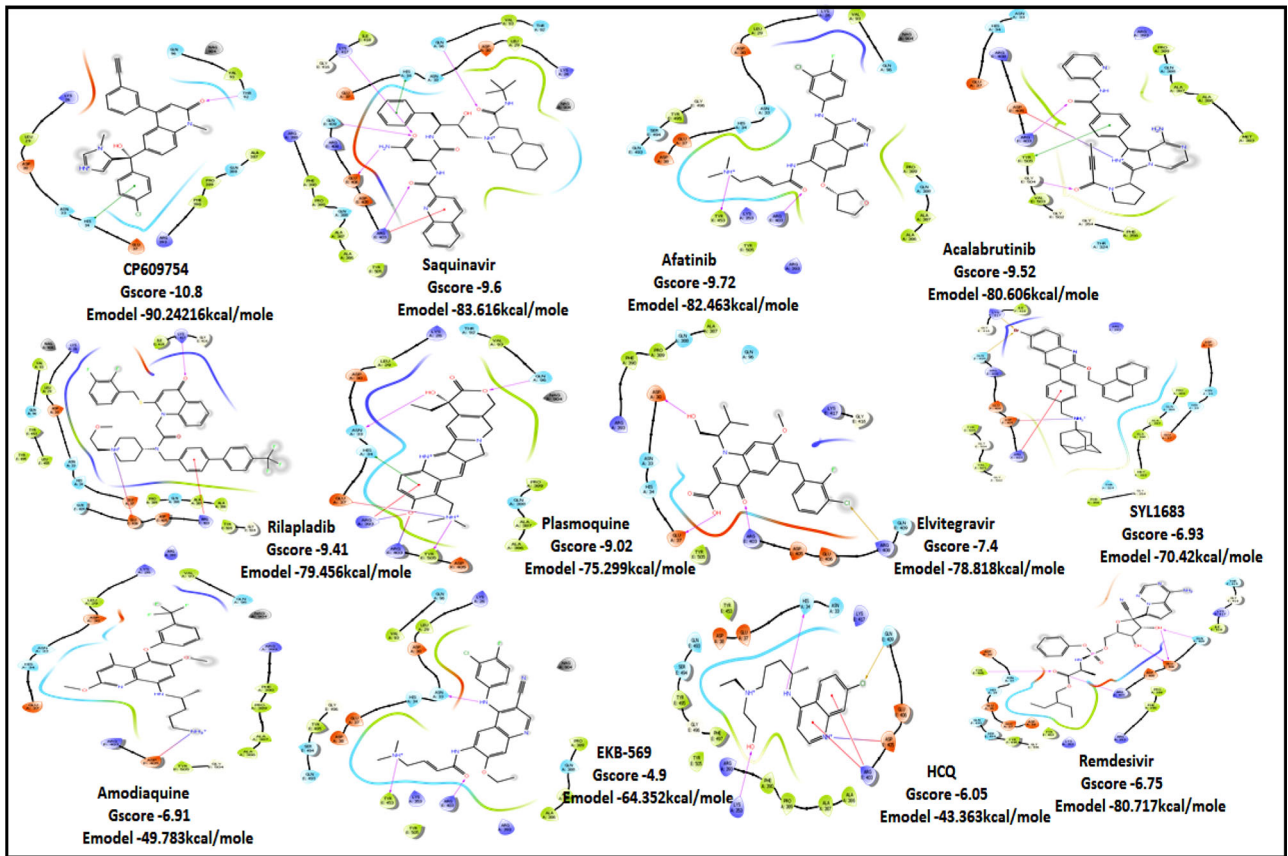


Figure 2. 2D Ligand Interaction Diagram for Top scores drugs to target RBD of SARS-COV-2.

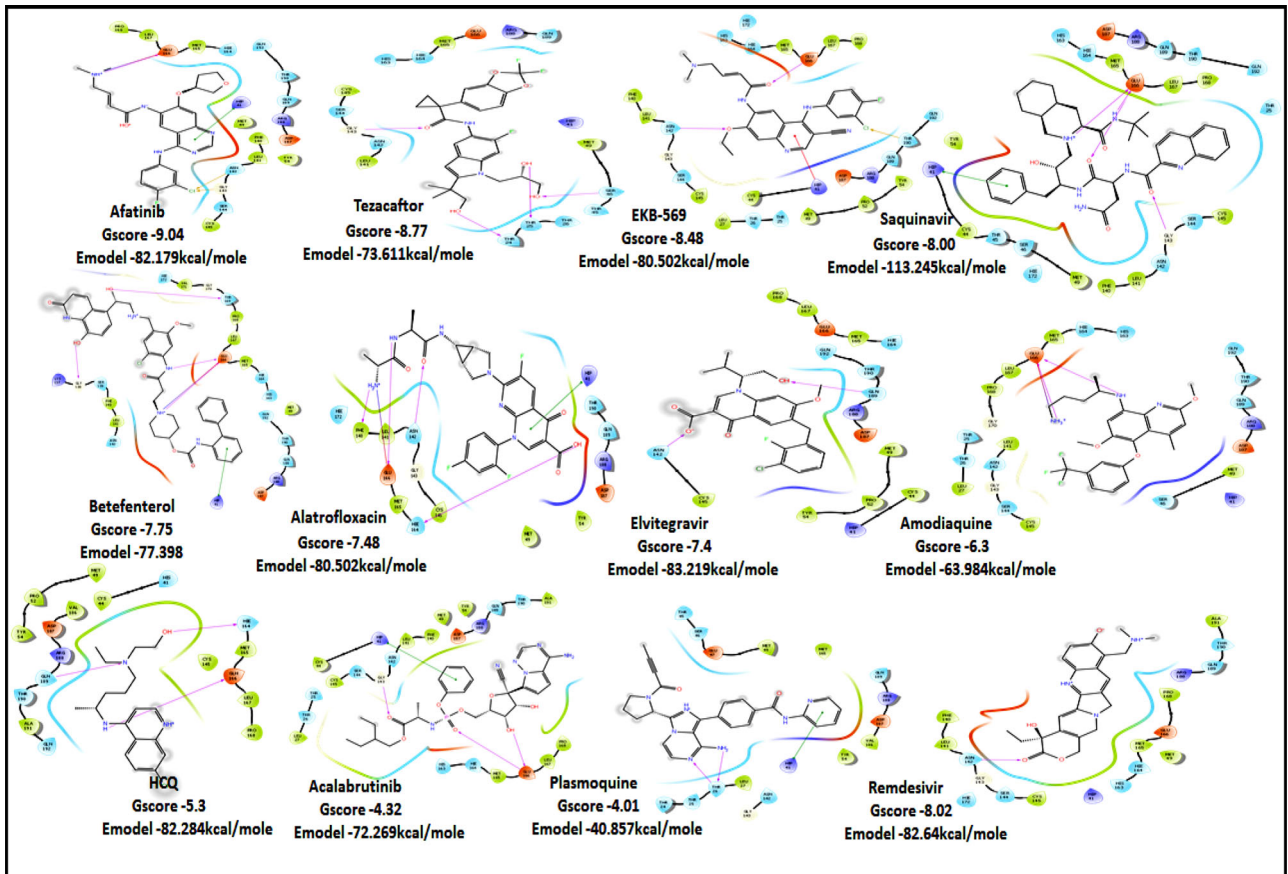


Figure 3. 2D Ligand Interaction Diagram for Top score drugs to target Main Protease of SARS-COV-2.

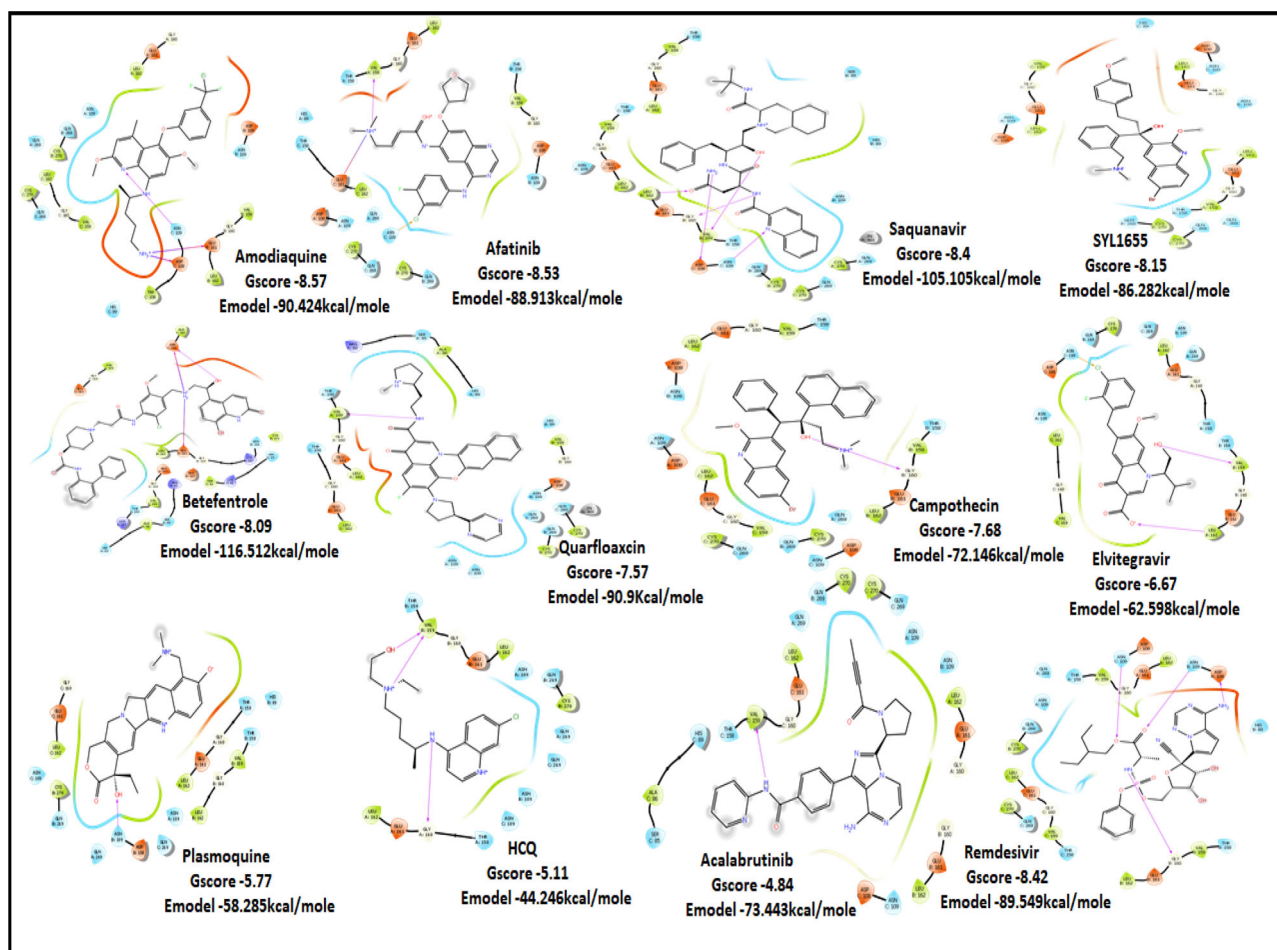


Figure 4. 2D Ligand Interaction Diagram for Top score drugs to target Papain Protease of SARS-COV-2.

have screened a total of hundred plus FDA approved quinoline based drugs. They are categorised based on their approved clinical application. (their detailed properties and mode of action are displayed in supplementary).

Five targets are used for this study:

Class 1: Targeting viral entry

Target 1: RBD S protein that provides a viral surface for the attachment to host cell receptor ACE2.

Class 2: Targeting viral replication

Class 2a: Replicase polyprotein

Target 2: M^{Pro} and PL^{Pro} both are responsible for proteolysis of viral polyprotein into functional unit.

Target 3: Papain-like proteases

Class 2b: Viral assembly

Target 4: Nucleocapsid proteins

Class 2c: Viral RNA synthesis by targeting RNA Dependent RNA Polymerase

Target 5: RdRp is responsible for replicating viral genome

Tables 1 and 2 summarizes the top-ranking compounds with their respective targets and their 2D Ligand Interaction Diagram (LID) are displayed in Figures 2–6.

3.1.1. Docking results for class 1, target 1: viral entry

The antivirals were the top scorers when averaged over the docking scores and energy (Figure 7(a)). Even though kinase inhibitors average values were lower, the top rankers included inhibitors with better potential like Afatinib, Acalabrutinib and Rilapladib.

RBD S protein is responsible for the entry of SARS-COV-2 into a host cell, which simultaneously binds with ACE2 and TMPRSS into the host cell. Therefore, targeting RBD Spike protein of SARS-COV-2 is the most prior step (Lan et al., 2020). Among all the screened drugs CP-609754 had the highest G-Score of -10.8 kcal/mol. The binding was approximately 78.51% higher than hydroxyquinoline (having a G-score of -6.05 kcal/mol). An insight into its binding highlight the additional hydrophobic energy due to the terminal propargyl group. However, not all the amino acids lining the binding pocket adds to the interaction, and the significant contributors are given in Table 3. A good ligand should have a combination of best fit and docking parameters. The next ranking molecules were Saquinavir and Afatinib, showing a G-score of -9.6 kcal/mol and -9.72 kcal/mol, respectively. Docking pose reveals a higher contribution from polar forces like the H bonding. Saquinavir and Afatinib have the best combination of both G-score and amino acid participation

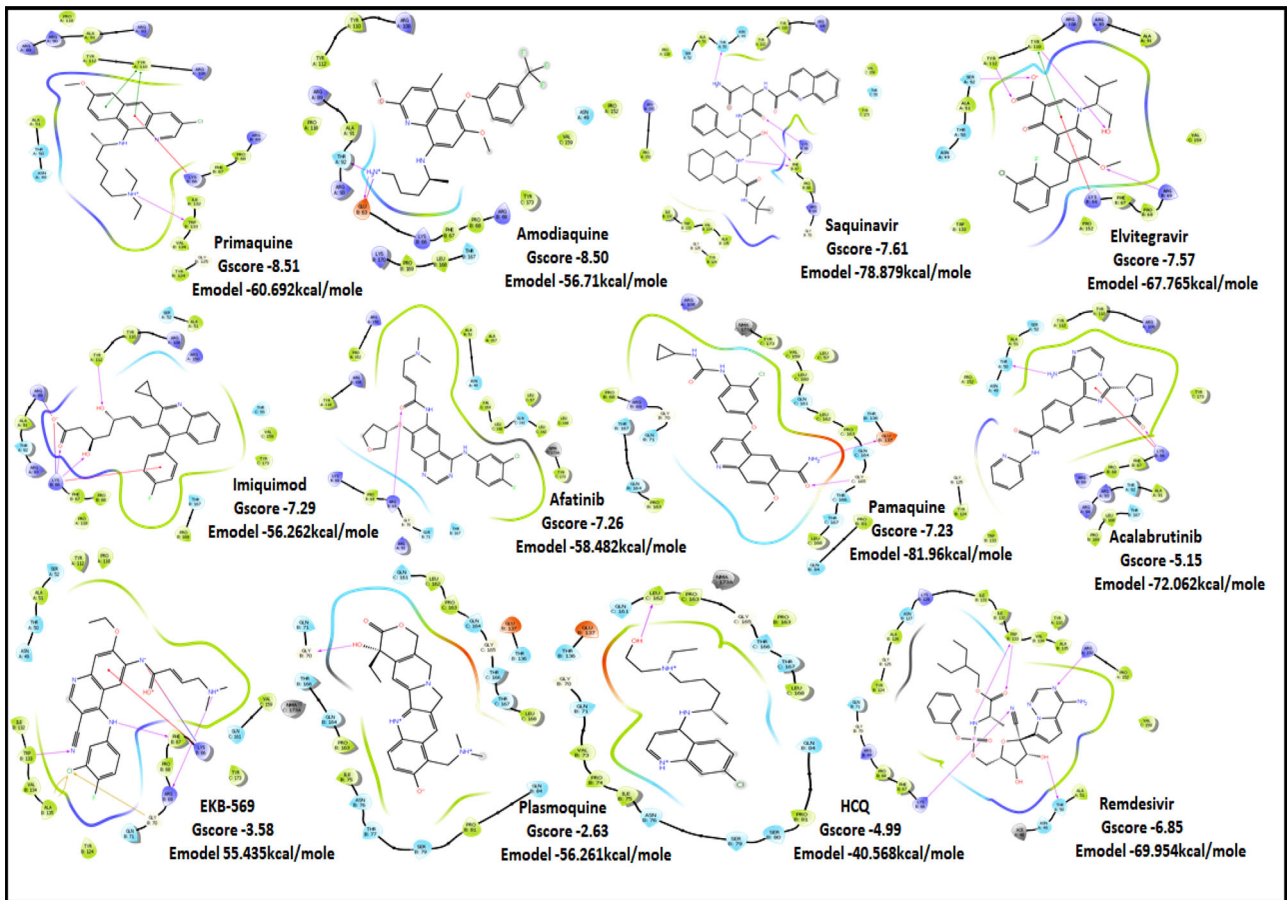


Figure 5. 2D Ligand Interaction Diagram for Top score drugs to target Nucleocapsid Protein of SARS-COV-2.

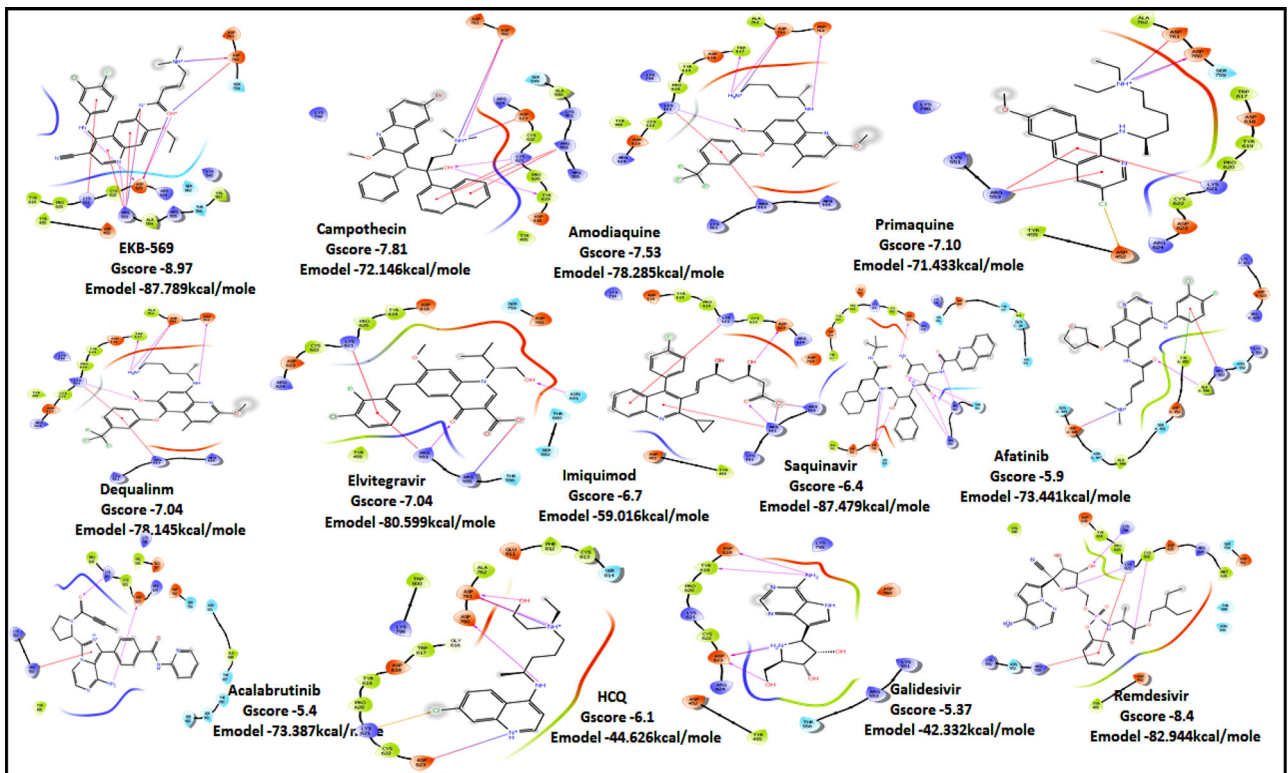


Figure 6. 2D Ligand Interaction Diagram for Top score drugs to target RNA dependent RNA polymerase of SARS-COV-2.

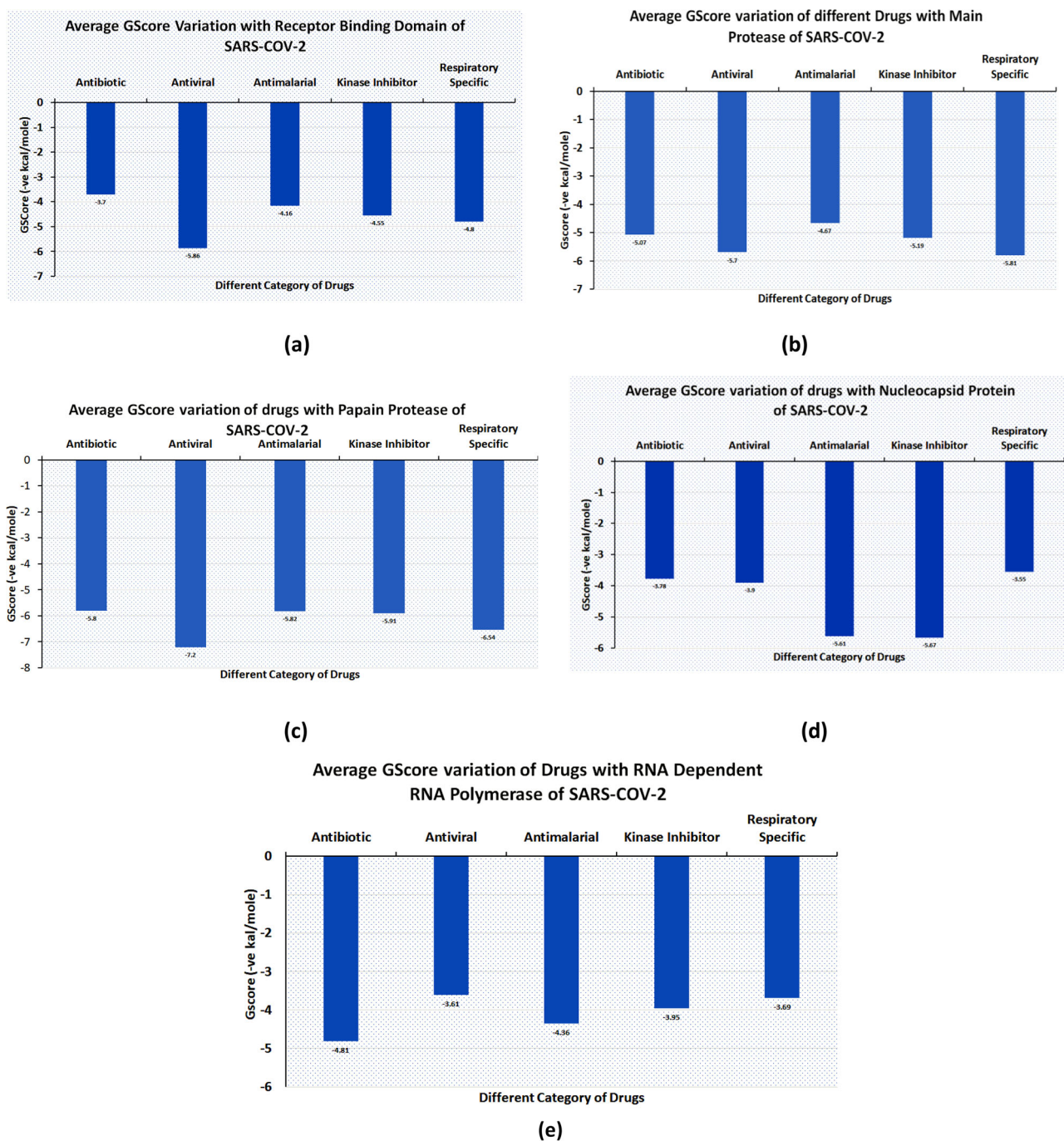


Figure 7. Average GScore variation for different category of Drugs with all therapeutics targets of SARS-COV-2 (Antimalarial, Antiviral, kinase inhibitor, Antiviral, Respiratory specific).

resulting in a better fit. Saquinavir has more fitting in the active site of binding pocket as there are five hydrogen bonds between heteroatoms of saquinavir and within the active site of RBD. Three oxygen forms hydrogen bonds with Gln96, Arg403, Gln406, Gln409 and Lys417. Also, the amine group of the alkyl chain forms a hydrogen bond with Glu406. Aromatic ring in saquinavir forms π - π stacking with Arg403. The residue in the active site with which saquinavir binds are Arg408, Lys417, Tyr505, Gly416, Ile418, which are crucial for binding with RBD of SARS-COV-2 (Sachdeva et al., 2020).

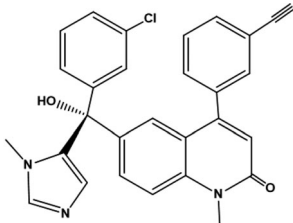
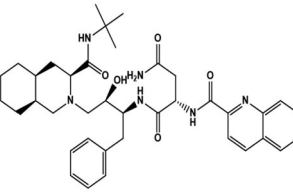
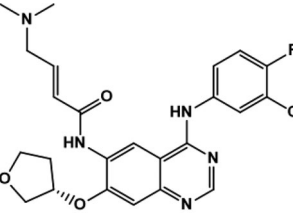
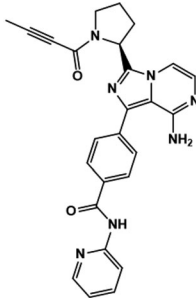
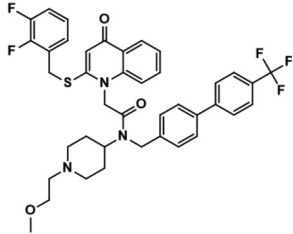
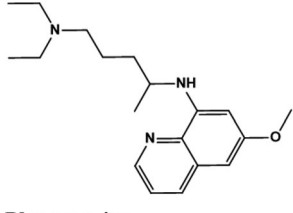
Acalabrutinib exhibited the G-score of -9.52 kcal/mol with key interactions between oxygen atoms and Arg403 and

Gly505 as H-bonding and π - π stacking of aromatic ring with Tyr505. The protonated nitrogen forms a salt bridge with Asp405.

Next in series were rilapladib and plasmoquine with G-score -9.41 kcal/mol and -9.02 kcal/mol (Docking Parameters Table 4). Rest of drugs details have provided in Table S7⁵¹.

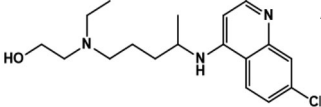
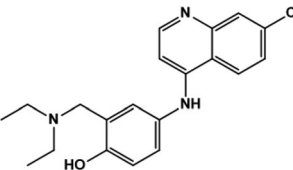
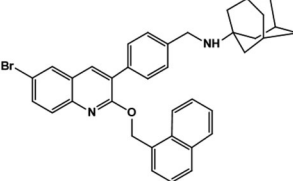
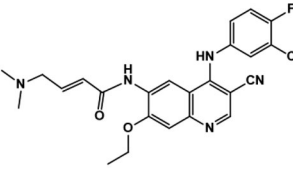
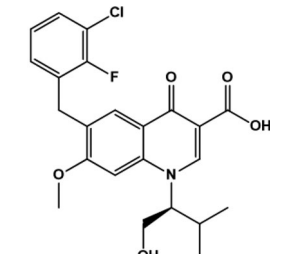
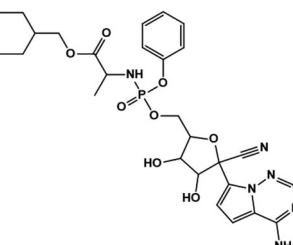
The screened drugs having a G-Score greater than 8.00 kcal/mol showed in general, the binding interactions with the following residues: H-bonding with Gln496, Lys417, and Arg408, pi-pi stacking with Tyr505, Tyr453, Tyr449, Glu37, Asp38, Lys68 are considered as potent drugs for blocking the Spike-ACE2 interactions.

Table 3. Interacting amino acids for Drugs with RBD of SARS-COV-2 (6M0J) with G-Score above Hydroxyquinoline and active side residue are marked bold.

Compound (6M0J)	Mode of Action	Hydrophobic	Polar	Hydrogen bonding	π - π stacking	Charged
 CP609754	Farnesyl transferase inhibitor	Val93, Leu29, Ala387, Pro389, Phe390	His33, Gln96, Thr92, Gln388		Thr92	Lys26, Asp30 , Glu37 , Arg393
 Saquinavir	Anti-HIV Protease inhibitor	Chain A: Phe390, Pro389, Ala387, Ala386, Val93, Leu29 Chain E: Tyr505 , Ile418 , Gly416	Chain A: Gln388, Asn33, Gln96, Thr92, Gln E: 409	Chain A: Gln96, Chain E: Lys417 , Gln409, Gln406, Arg403	Chain E Arg403,	Chain A: Glu37 , Arg393, Asp30 , Lys26 Chain E: Glu406, Asp405, Arg403, Arg408 , Lys417
 Afatinib	Tyrosine Kinase inhibitor; Epidermal Growth Factor Receptor (EGFR) inhibitor	Chain A: Ala387, Ala386, Leu29, Val93, Pro389 Chain E: Tyr495, Gln496 , Tyr453	Chain A: His33, Gln388, Gln96 Chain E: Gln 493, Ser494		Chain E: Tyr 453 , Arg403,	Chain A: Glu37 , Asp38 , Asp30 , Lys353 , Lys26, Arg393 Chain E: Arg403,
 Acalabrutinib	Bruton Tyrosine Kinase Inhibitor	Chain A: Pro389, Ala387, Ala386, Met383, Gly354, Phe356 Chain E: Tyr505 , Gly504, Val503, Gly502	Chain A: Asn33, Gln388, Thr324	Chain E: Gly504 , Arg403, Asp405	Chain E: Tyr505	Chain A: Glu37 , Arg393 Chain E: Asp405 , Arg408 , Arg403,
 Rilapladib	Lipoprotein associated phospholipase (A ₂) Lp-plA2 Inhibitor	Chain A: Pro389, Ala387, Phe390, Ala386, Leu29, Val93 Chain E: Tyr505 , Leu455, Gly504	Asn33, Gln388, Thr92, Gln96	Chain A: Asp30	Chain E: Arg403	Chain A: Asp30 , Lys26, Arg393 Chain E: Lys417, Arg408 , Arg403
 Plasmoquine	Synthetic Antimalarial Drug	Chain A: Pro389, Ala387, Ala386, Val93, Leu 29 Chain E: Tyr505	Chain A: Asn33, Gln388, Thr92, Gln96	Chain A: Asn33, Gln96, Arg393, Glu37 Chain E: Tyr505 , Arg403	Chain A: Arg393, Asn33	Chain A: Lys26, Asp30 , Glu37 , Arg393, Chain E: Arg403 , Asp405

(continued)

Table 3. Continued.

Compound (6M0J)	Mode of Action	Hydrophobic	Polar	Hydrogen bonding	π - π stacking	Charged
	Antimalarial Drug Anti-arthritis	Chain E: Tyr453 , Tyr495 , Gln496 , Phe497 , Tyr505 Chain A: Phe390 , Pro389 , Ala387 , Ala386	Chain E: Ser494 , Gln493	Chain A: Lys353 , Chain E: Asp405	Chain E: Arg403	Chain A: Asp38 , Glu37 , Arg393 , Lys353 , Chain E: Arg403 , Asp405 , Glu406
Hydroxyquinoline						
	Antimalarial Drug	Chain A: Leu29 , Val93 , Phe390 , Pro389 , Ala387 , Ala386 Chain E: Gly504 , Tyr505	Chain A: Asn33 , Gln96	Chain E: Asp405		Chain A: Lys26 , Arg393 , Asp30 , Glu37 Chain E: Arg403
Amodiaquine						
	Anti-HIV Inhibitor	Chain A: Pro389 , Ala387 , Ala386 , Met383 , Phe356 , Gly354 Chain E: Tyr505 , Gly504 , Val503 , Gly502 , Ile418 , Gly416	Chain A: Asn33 , Gln388 , Thr324 Chain E: Gln409	Chain E: Asp405 , Arg403 , Lys417 , Gln409	Chain E: Asp405 ,	Chain E: Lys417 , Arg408 , Arg403 Chain A: Arg393
SYL1683						
	Potent Irreversible EGFR receptor	Chain A: Leu29 , Val93 , Phe390 , Pro389 , Ala387 , Ala386 Chain E: Tyr505 , Tyr495 , Gly496 , Tyr453	Chain A: Asn33 , Gln96 , Gln388 Chain E: Ser494 , Gln493	Chain E: Arg403 , Tyr453 Chain A: Asn33		Chain A: Asp30 , Lys26 , Arg393 , Lys353 , Glu37 , Asp38 Chain E: Arg403
EKB-569						
	Anti-HIV Inhibitor	Chain A: Pro389 , Ala387 , Phe390 Chain E: Tyr505	Chain A: Asn33 , Gln388 , Gln96 Chain E: Gln409	Chain A: Asp30 , Glu37 Chain E: Arg403	Chain E: Arg408	Chain A: Asp30 , Glu37 , Arg393 Chain E: Lys417 , Arg408 , Arg403 , Asp405 , Glu406
Elvitegravir						
	Antiviral Drug	Chain A: Pro389 , Phe390 Chain E: Tyr505 , Tyr495 , Gly496 , Tyr453 , Ile418 , Gly416	Chain A: Asn33 , Chain E: Ser494 , Gln493 , Tyr415	Chain A: Asp30 Chain E: Glu406 , Gln409 , Tyr505 , Arg403		Chain A: Asp30 , Glu37 , Glu35 , Asp38 Arg393 , Lys353 Chain E: Lys417 , Arg403 , Asp405 , Glu406
Remdesivir						

3.1.2. Docking results for targets of Class 2: Replication Target 1: Interaction analysis within active site of SARS-COV-2 main protease M^{Pro} (three PDB IDs: 5R80- complexed with Z18197050, 6WTT-complexed with inhibitor GC376, 6LU7-with inhibitor N3)

When the quinoline library was docked on M^{Pro} PDB (5R80), and the average docking scores and binding energies compared, respiratory specific and antivirals emerged as most promising (Figure 7(b)).

M^{Pro} or the chymotrypsin like protease (3CLpro)/C30 Endopeptidase produces non-structural proteins that later play a role in mediating the replication of the virus (Elzupir, 2020). Therefore, inhibiting the activity of this enzyme can block viral replication. Once inside the host cell, the proteases of the virus cleave the mRNA into structural and non-structural proteins. The protease belongs to cysteine protease family with cysteine-histidine catalytic dyad. 3CLpro monomer has three domains, domain I (residues 8-101),

Table 4. Docking Parameters for Highest scoring drugs with receptor binding domain of SARS-COV-2 (PDB ID 6M0J).

Drugs	GScore	DScore	Lipophilic EVDW	Hbond	EModel
CP609754	-10.8	-8.26	-6.23	-2.34	-90.242
Saquinavir	-9.6	-8.32	-4.46	-1.96	-83.616
Afatinib	-9.72	-7.24	-4.39	-1.45	-82.436
Acalabrutinib	-9.52	-8.73	-3.3	-1.1	-80.606
Rilapladib	-9.41	-8.24	-4.89	-0.29	-79.456
Plasmaquine	-9.02	-8.13	-6.23	-2.6	-75.299
Elvitegravir	-7.4	-7.2	-5.23	-1.3	-78.818
Amodiaquine	-6.91	-5.64	-3.15	-1.08	-49.763
SYL1683	-6.93	-5.92	-4.25	0	-70.42
Remdesivir	-6.75	-6.75	-5.22	-2.73	-80.717
HQ	-6.05	-5.64	-3.15	-1.08	-43.363
EKB-569	-4.9	-4.4	-4.4	-1.1	-64.352

	Tezacaftor	Afatinib	Acarabrutinib	EKB-569	Primaquine	Rilapladib	Amodiaquine	HCQ
Absorption								
Caco-2	-	-	-	-	+	-	+	+
Human Intestinal Absorption	+	+	+	+	+	+	+	+
P-glycoprotein inhibitor	0.7316	0.9009	0.8277	0.8458	0.9252	0.8755	0.6678	0.7900
P-glycoprotein substrate	+	+	+	+	+	+	+	+
	0.6446	0.5191	0.6331	0.5650	0.7846	0.7717	0.6470	0.9103
Distribution								
Blood Brain Barrier	+	+	+	+	+	+	+	+
	0.9670	0.9783	0.9928	0.9793	0.9894	0.9818	0.9822	0.9878
Subcellular localization	Mitochondria	Mitochondria	Mitochondria	Mitochondria	Nucleus	Mitochondria	Lysosomes	Lysosomes
Metabolism								
CYP2D6 inhibition	-	-	-	-	+	-	+	-
	0.7072		0.8909	0.8182	0.8932	0.9237	0.7582	0.6111
CYP2D6 substrate	-	-	-	-	+	-	+	-
	0.8230	0.7895	0.8831	0.8182	0.5523	0.7913	0.3783	0.4601
CYP3A4 inhibition	+	-	-	+	-	+	-	-
	0.7381	0.6846	0.5071	0.6233	0.8310	0.5648	0.7203	0.6287
CYP3A4 substrate	+	+	+	+	-	+	+	+
	0.6467	0.7171	0.6434	0.7339	0.5334	0.7483	0.5640	0.6652
CYP inhibitory promiscuity	+	+	+	+	-	+	+	-
	0.8695	0.7096	0.6607	0.8580	0.5057	0.7996	0.9292	0.7058
OATP1B1 inhibitor	+	-	+	+	+	+	+	+
	0.8944	0.8400	0.9132	0.8708	0.9605	0.8832	0.9241	0.9290
OATP1B3 inhibitor	+	+	+	+	+	+	+	+
	0.9318	0.9421	0.948	0.9429	0.9647	0.9406	0.9427	0.9431
Excretion								
OCT2 inhibitor	-	-	-	-	+	-	-	-
	0.8537	0.6109	0.5000	0.6500	0.8250	0.5000	0.7000	0.5000
MATE1 inhibitor	-	-	-	-	-	-	-	-
	0.8619	0.9400	0.8000	0.8400	0.9800	0.6200	0.8400	0.8600
Toxicity								
Carcinogenicity (binary)	-	-	-	-	-	-	-	-
Eye corrosion	-	-	-	-	-	-	-	-
Eye irritation	-	-	-	-	-	-	-	-
Acute Oral Toxicity (c)	III	III	III	III	III	III	III	III

Figure 8. ADME Properties of top-ranking drugs (*red for toxicity and inhibitor, *green for safety and non-inhibitor and *orange for less toxic).

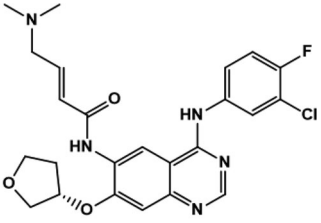
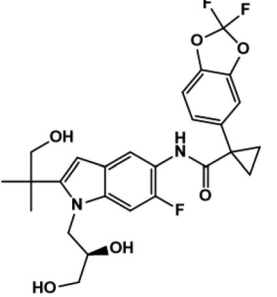
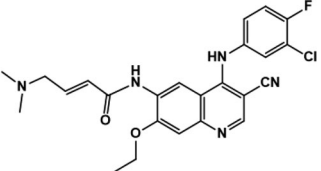
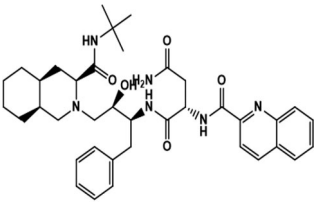
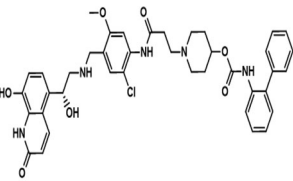
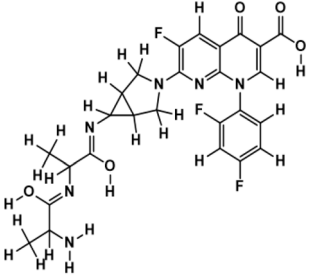
domain II (residues 102-184) and domain III (residues 201-303), and a long loop (residues 185-200) connects domains II and III. The active site of 3CLpro is located in the gap between domains I and II, and has a Cys-His catalytic dyad (Cys145 and His41 (Vatansever et al., 2020)). Recently, aminoquinolines have been reported as inhibitors of certain cysteine proteases (Braga et al., 2017). However, a greater number of antivirals and inhibitors scored above hydroxyquinoline. Only tezacaftor, that is a cystic fibrosis transmembrane conductance regulator (CFTR) was able to score a higher G-Score.

Molecules with docking scores more than that of hydroxyquinoline (G-score -5.4) are summarised in the Table 1. Ligand Interaction Diagram for top scorers with 5R80 are

shown in Figure 3 and their interaction information are provided in Table 5). Afatinib has the best G-score of -9.04 kcal/mol, followed by tezacaftor G-score of -8.77 kcal/mol (Docking Parameters) (Table 6). Table G-score of rest of drugs have represented in Table S8^{S1}.

Among all the drugs, afatinib with GScore -9.04 was well fitted into the binding pocket of M^{Pro} and the binding was 67.4% higher than that of HCQ. A similar trend was observed when the molecules were docked on other PDBs of M^{Pro} (6WTT, 6LU7). Afatinib was the top scorer with GScore of -9.3 kcal/mol with 6WTT and -9.943 kcal/mol with 6LU7 and also showed binding with catalytic dyad forming π - π stacking with Hip41 and interaction with Cys145. The binding pocket is primarily

Table 5. Ligand Interaction information for top scoring drugs to inhibit the activity of main protease of SARS-COV-2 (5R80).

Compound	Mode of Action	Hydrophobic	Polar	π - π stacking	H-Bond	Charged
 <p>Afatinib</p>	Tyrosine Kinase inhibitor; Epidermal Growth Factor Receptor (EGFR) inhibitor	Phe140, Leu141, GLY143, Cys145, Leu27, Cys44, Tyr54, Pro52, Met49, Met165, Leu167, Pro168	Asn142, Ser144, Thr26, Thr25, His163, Hie164, Gln189, Thr190, Gln192	Glu166		Hip41 Asp187 Arg188 Glu166
 <p>Tezacaftor</p>	Cystic Fibrosis Transmembrane Conductance regulator	Leu141, Gly143 Cys145, Met49 Met165	Gln189, Hie164, His163, Gln189, Hie164, His163, Ser46	Gly143, Thr25, Thr24, Ser46		Hip41, Arg188, Glu166
 <p>EKB-569</p>	An irreversible Epidermal Receptor Growth receptor Tyrosine kinase	Phe140, Leu141, Gly143, Cys145, Met165, Cys44, Met49, Pro52, Tyr54	Hie172, Asn142, Ser144, Thr190, Gln189, Gln192, Thr25, Hie164, His163	Glu166, Thr190	Hip41	Hip41 Asp187 Arg188 Glu166
 <p>Saquinavir</p>	Anti-HIV Protease inhibitor	Tyr54, Cys44, Met49, Phe140, Leu141, Cys145, Met165, Leu167, Pro168	Thr45, Ser46, Hie172, Asn142, Ser144, Thr25, His163, Hie164	Glu166	Hip41	Hip41 Asp187 Arg188 Glu166
 <p>Batefenterol</p>	α_2 adrenoceptors agonist, muscarinic receptor antagonist	Leu167, Met165, Pro168, Phe140, Leu141, Met49, Gly170, Gly138, Val171	Gln189, Hie164, Thr190, His163, Gln192, Thr169, Hie172, Ser139, Asn142	Gly138, Glu166, Thr169	Hip41	Hip41, Arg188, Asp187, Glu166
 <p>Alatrofloxacin</p>	Antibacterial Antineoplastic DNA topoisomerase inhibitor	Phe140, Leu141, Cys145, Gly143, Met49, Tyr54	Gln189, Thr190, Hie164, Asn142, Hie172	Glu166, Asn142, Phe140, Hie164, Glu166	Hip41	Hip41, Arg188, Asp187, Glu166

(continued)

Table 5. Continued.


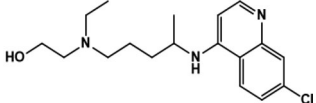
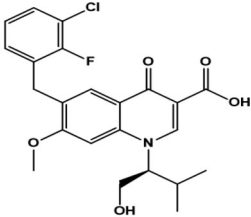
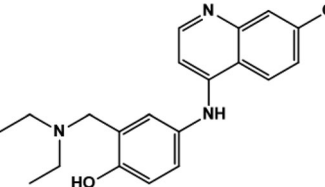
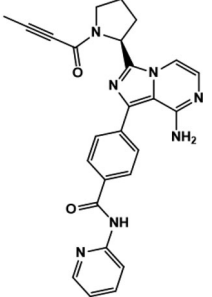
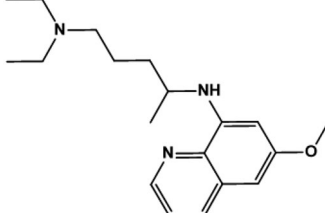
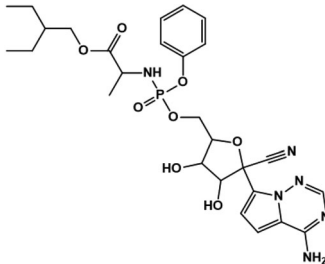
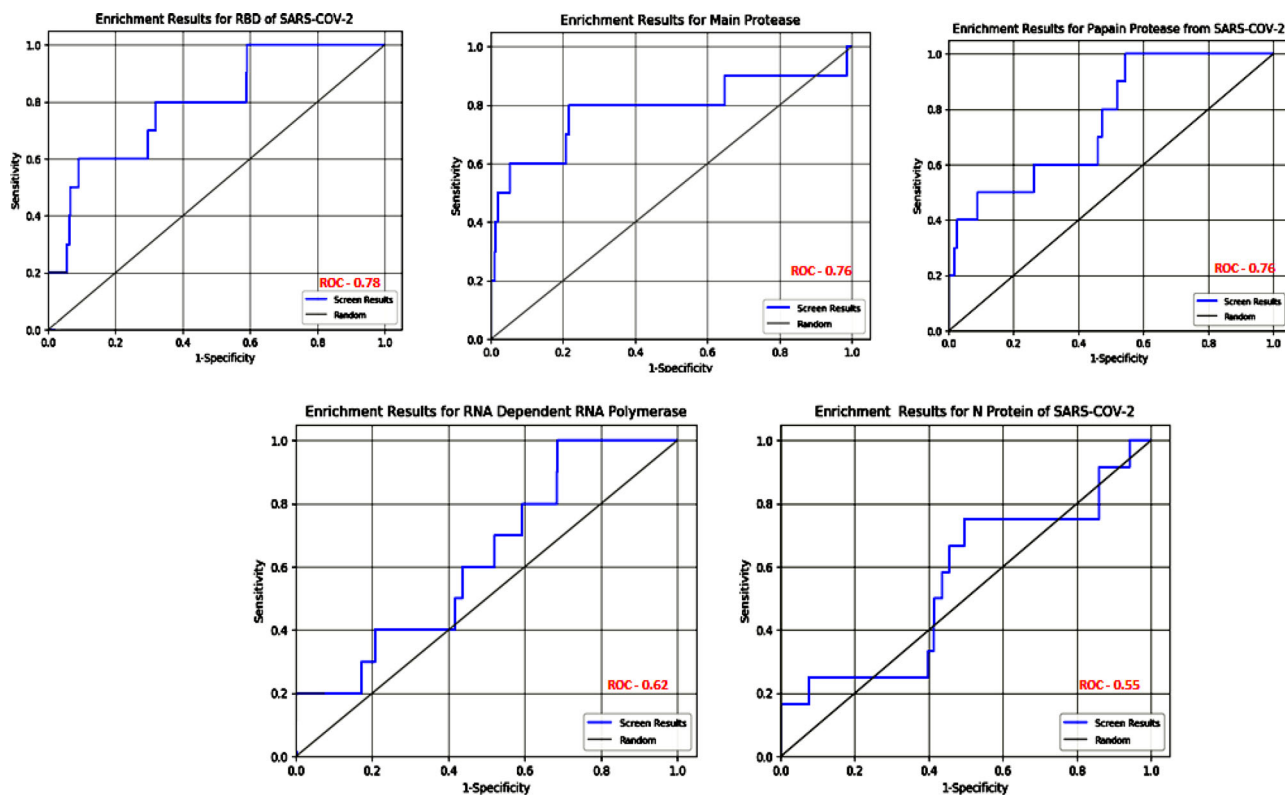
Compound	Mode of Action	Hydrophobic	Polar	π - π stacking	H-Bond	Charged
		Pro168, Leu167, Met165, Met49, Cys44, Tyr54	Gln189, Thr190, Gln192			Hip41, Arg188, Asp187, Glu166
Co-crystallized Z1819750						
	Antimalarial Drug Anti-arthritis	Cys145, Met165, Gly143, Leu141, Phe140, Tyr54, Pro52, Met49, Cys44	Hie164, His163, Ser144, Asn142	Glu166	Hip41	Hip41, Arg188, Asp187, Glu166
Hydroxychloroquine						
	Anti-HIV Inhibitor	Pro168, Leu167, Met165, Val186, Tyr54, Pro52, Met49, Cys44, Cys145	Gln189, Thr190, Gln192, Hie164, Asn142	Hie164		Hip41, Arg188, Asp187, Glu166
Elvitegravir						
	Antimalarial Drug	Met49, Leu27, Pro168, Leu167, Met165, Gly170, Leu141, Gly143	Gln189, Thr190, Gln192, Hie164, His163, Asn142, Hie172, Ser144, Thr25, Thr26	Glu166		Hip41, Arg188, Asp187, Glu166
Amodiaquine						
	Tyrosine Kinase inhibitor; Epidermal Growth Factor Receptor (EGFR) inhibitor	Leu167, Met165, Pro168, Met49, Tyr54, Cys44, Gly143, Cys145	Gln192, Gln189, Thr190, Hie164, Ser46, Thr45, Thr25	Gln189, Arg188		Hip41, Arg188, Asp187, Glu166
Acalabrutinib						
	Antimalarial Drug	Met165, Pro168, Met49, Phe140, Leu141, Gly143, Cys145	Gln189, Thr190, Hie164, His163, Ser144, Asn142, Hie172	Asn142		Hip41, Arg188, Glu166
Plasmoquine						
	Antiviral Drug	Ala191, Pro168, Phe140, Leu141, Cys145, Met49, Met165, Gly143	Gln189, Thr190, Hie164, His163, Ser144, Asn142, Hie172	Asn142		Glu166, Arg188, Hip41
Remdesivir						

Table 6. Docking Parameters for top scoring drugs with main protease of SARS-COV-2 (PDB ID 5R80).

Drugs	GScore	DScore	Lipophilic EVDW	Hbond	EModel
Afatinib	-9.04	-7.86	-5.44	-2.03	-82.179
Tezacaftor	-8.77	-8.77	-3.44	-3.75	-73.611
EKB-569	-8.48	-7.29	-4.91	-0.6	-80.502
Saquinavir	-8.0	-8.32	-4.46	-1.96	-113.245
Batefeneterol	-7.75	-6.95	-3.46	-0.56	-77.398
Alatrofloxacin	-7.48	-6.23	-3.73	-2.9	-80.502
Elvitegravir	-7.4	-7.2	-5.23	-1.3	-83.219
Amodiaquine	-6.3	-6.3	-4.52	-1.57	-63.984
Remdesivir	-8.02	-8.018	-5.22	-2.73	-82.640
HQ	-5.3	-5.2	-1.2	-0.6	-82.284
Acalabrutinib	-4.32	-4.31	-3.85	-0.82	-72.269
Plasmaquine	-4.01	-3.78	-3.85	-0.5	-40.857

**Figure 9.** Receiver Operator Characteristics Curve for all active drugs with therapeutics targets of SARS-COV-2.

marked by the catalytic dyad of amino acids Cys145 and His41 (Khan et al., 2020). All reported residues in the active site of binding pocket of M^{Pro} and as evident in the co-crystallized PDB bind to afatinib. The quinoline ring in afatinib showed π - π stacking with Hip41 along with the H-bond between protonated nitrogen with Glu166 and covalent interaction of chlorine atom with Asn142 and Gly143. Also, afatinib bind with 12 Hydrophobic residues and with ten polar residues. Therefore, afatinib can be considered the potent drug for targeting main protease of SARS-COV-2.

3.1.3. Target 3: Interaction characterization of quinoline based drugs with SARS-COV-2 papain like protease

When the quinoline library was docked on PL^{Pro} PDB (6W9C), averaged G-scores, docking scores and binding energies were compared, respiratory specific are served as most promising (Figure 7(c)).

PL^{Pro} is responsible for the cleavages of N-terminus of the replicate poly-protein to release non-structured proteins (Nsp1-3), essential for correcting virus replication. PL^{Pro} was also confirmed to be significant in antagonizing the innate immunity of the host. As an indispensable enzyme in the process of coronavirus replication and infection of the host, PL^{Pro} has been a popular target for coronavirus inhibitors. It is very valuable for targeting PL^{Pro} to treat coronavirus infections, but no inhibitor has been approved by the FDA for marketing. All quinoline based drugs were docked with crystal structure of PL^{Pro} (PDB ID 6W9C). Docking Parameters for high scoring drugs are displayed in Table 7. Remdesivir was considered as control with GScore of -8.4 kcal/mol. Among all screened drugs again, amodiaquine, afatinib and saquinavir having G-scores -8.57 , -8.53 and -8.4 respectively scored above remdesivir. The binding pocket is primarily marked by the amino acids Gly270, Asp103, Gly164 and their interaction information are provided in Table 8. Heteroatoms

Table 7. Docking parameters of top scorer drugs to target papain protease of SARS-COV-2 (PDB ID 6W9C).

Drugs	GScore	DScore	Lipophilic EVDW	HBond	EModel
Amodiaquine	-8.57	-8.56	-5.34	-1.62	-90.424
Afatinib	-8.53	-7.49	-5.22	-0.32	-88.913
Saquinavir	-8.4	-8.38	-5.78	-1.99	-105.105
SYL1655	-8.15	-8.11	-7.76	-0.48	-86.282
Batefenterol	-8.09	-8.03	-5.23	-1.49	-116.512
Quarflorin	-7.57	-7.57	-6.87	-0.7	-90.9
HCQ	-5.11	-5.06	-3.76	-0.7	-44.246
Remdesivir	-8.42	-8.42	-5.57	-2.29	-89.549
Campothecin	-7.68	-7.68	-6.52	-0.42	-72.146
Elvitegravir	-6.67	-6.54	-5.27	-1.05	-62.598
Plasmaquine	-5.77	-5.54	-4.44	-0.85	-58.285
Acalabrutinib	-4.84	-4.82	-4.72	-0.04	-73.443

of amodiaquine viz., protonated nitrogen and nitrogen atom of quinoline ring form H-bond with Asn109, Asp108, Val159 and Glu161. Other residues in the binding pocket of PL^{Pro} with Amodiaquine forms covalent interaction are Cys270, Leu162, Trp106, Val159, Gly160.

Ligand Interaction Diagram for top scorers with 6W9C are displayed in Figure 4. Docking parameters for rest of drugs with 6W9C are provided in Table 9^{*S1}.

3.1.4. Target 4: Interaction characterization of quinoline based drugs with RNA binding domain of nucleocapsid protein of SARS-COV-2

When the quinoline library was docked on PDB (6M3M), average GScore and the average docking scores and binding energies compared, respiratory specific drugs emerged as most promising (Figure 7(d)).

The SARS-COV-2 nucleocapsid RNA binding protein plays a vital role in viral RNA transcription and replication. As the name is suggestive of its function, the primary function of the N-protein is binding to the viral RNA genome and packing into a long helical nucleocapsid structure or ribonucleoprotein (RNP) complex (Dutta et al., 2020). Experimental studies revealed that N-protein maintains highly ordered RNA conformation suitable for replicating and transcribing the viral genome. The protein is speculated to regulate host-pathogen interactions, such as actin reorganization, host cell cycle progression, and apoptosis. The N protein itself is highly immunogenic and abundantly expressed protein during infection, capable of inducing protective immune responses against SARS-CoV-2 (Kang et al., 2020).

The docking Parameters and Ligand Interaction amino acids are provided in Tables 9 and 8 respectively. The drugs that have GScore greater than or equal to -7 are considered best candidates and bind with residues Ala51, Tyr112, Tyr124 within the active site are considered potent drugs for targeting N protein. Docking with Nucleocapsid proteins of SARS-COV-2 suggest that primaquine and amodiaquine antimalarial drugs serve as the best inhibitor with G-score -8.5, followed by saquinavir with GScore -7.61 kcal/mol and elvitegravir with -7.57 kcal/mol respectively (Table 1). Key interactions are the H-bond between protonated nitrogen atom in primaquine and Trp133, π - π stacking with Tyr110 and Lys66, and covalent interactions with Ala51, Thr50, Asn49, Ty124 and Tyr110, which are crucial for binding with RNA binding domain of N Protein,

and makes it the best drug to target Nucleocapsid protein of SARS-COV-2. The GScore of primaquine is 70.2% higher than HCQ. Ligand Interaction Diagram for top scorers are displayed in Figure 5 with 6M3M. Docking parameters for rest of drugs with 6M3M are provided in Table S10^{*S1}.

3.1.5. Target 5: Interaction characterization of quinoline based drugs with SARS-COV-2 RNA dependent RNA polymerase (PDB ID 7BTF)

The quinoline library was docked on PDB (7BTF), and the average docking scores and binding energies compared kinase inhibitors emerged as most promising (Figure 7(e)).

RDRP is a vital enzyme for the life cycle of the single-stranded RNA coronavirus (Elfiky, 2020). The function of RdRp is to convert a single-stranded RNA virus into many single-stranded RNA viruses. RdRp active site is conserved among different organisms, while two successive, surface-exposed aspartate residues are protruding from a beta-turn motif (Yin et al., 2020).

Ligand Interaction Diagram for top scorers with 7BTF are displayed in Figure 6. The binding pocket is primarily marked by the amino acids Asp760 and Asp761. As galidesivir is considered as the best ligand for RdRp, it was used as a control with a GScore of -5.375 kcal/mol. Docking with RdRp suggests that EKB-569 has the highest binding with GScore value -8.97 kcal/mol followed by campothecin with GScore -7.81 kcal/mol. The docking parameters and interaction amino acids informations are provided in Tables 11 and 12 respectively. The binding of EKB-569 with RdRp was approximately 66.8% higher than that of galidesivir. The protonated nitrogen and oxygen atoms of EKB-569 form hydrogen bonding with Asp760 and Asp761, which is crucial for binding within the active site of RNA dependent RNA polymerase from SARS-COV-2. The interactions also include π - π stacking between the aromatic and quinoline rings with Lys621, Arg553, and a hydrogen bond with Arg553.

The drugs having GScore greater than or equal to -7.00 kcal/mol and bind with active site residue Asp760 and Asp761 within the active site are considered as potent drugs to target RdRp from SARS-COV-2

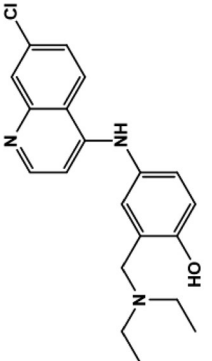
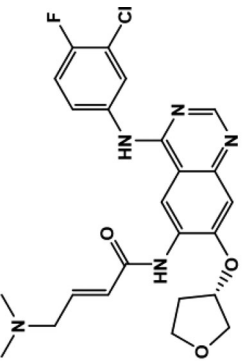
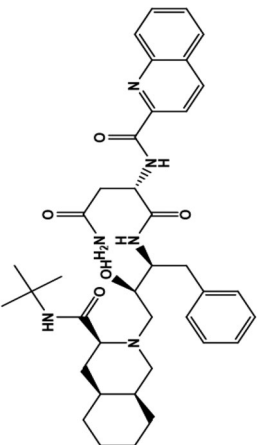
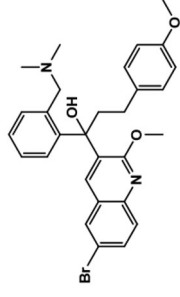
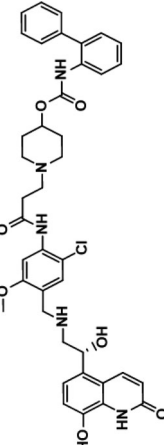
Ligand Interaction Diagram for top scorers with 7BTF are displayed in Figure 6. Docking parameters rest of drugs with 7BTF are provided in Table S11^{*S1}.

A preliminary analysis based on higher score than the control hydroxyquinoline (Table 1) reflects the following. Overall, among all the drugs amodiaquine serves as best for all the targets. Afatinib and saquinavir were above the HQ in four of the targets. This analysis brings out the contenders that may target multiple targets. Elvitegravir and EKB-569 reserved their roles as inhibitors of proteases and RdRp polymerase. Rilapladib emerged as a potential candidate for inhibition of viral entry with binding potential with ACE2 (Tables 11 and 12).

3.3. In silico ADME properties

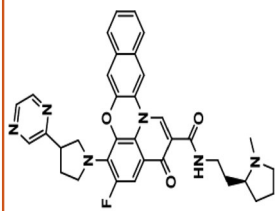
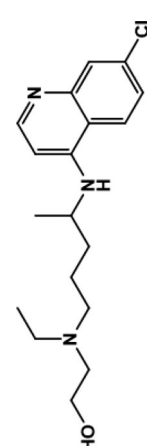
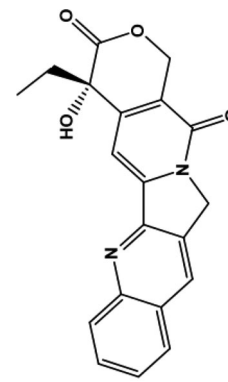
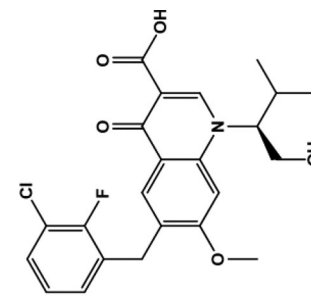
The compilation of bioactivity parameters is presented in Table S6^{*S1}. Results of in silico ADME analysis indicate the following results: (Figure 8)

Table 8. Interacting amino acids for Drugs having G-Score above Hydroxyquinoline for Papain Protease of SARS-COV-2 (PDB ID: 6W9C).

Compound	Mode of Action	Hydrophobic	Polar	π-π Stacking	H-Bond	Charged
 Amodiaquine	Antimalarial, Anti-inflammatory	Chain A: Gly160, Leu162 Chain B: Leu162, Val159, Cys270, Gly160 Chain C: Leu162, Val159, Gly160, Trp106, Cys270	Chain A: Asn109, Gln269 Chain B: Asn109, Gln269 Chain C: Asn109, His89, Gln269	Chain B: Glu161 Chain C: Asn109, Asp108		Chain A: Glu161 Chain B: Glu161, Asp108 Chain C: Asp108
 Afatinib	Tyrosine Kinase inhibitor; Epidermal Growth Factor Receptor (EGFR) inhibitor	Chain A: Val159, Gly160, Leu162 Chain B: Val159, Gly160, Trp106, Cys270 Chain C: Val159, Leu162, Gly160, Cys270	Chain A: Asn109, Gln269, Thr158 Chain B: Asn109, Gln269, His89 Chain C: Thr158, Gln269, Asn109		Chain C: Asn109	Chain A: Glu161, Chain B: Asp108, Chain C: Glu161
 Saquinavir	Anti-HIV Protease inhibitor	Chain A: Leu162, Val159, Gly160 Chain B: Leu162, Val159, Cys270 Chain C: Leu162, Val159, Cys270, Gly160	Chain A: Thr158, Asn109, Gln269 Chain B: Thr158, Asn109, Gln269, His89, Ser85 Chain C: Thr158, Asn109, Gln269	Chain B: Leu162, Val159, Gly160 Chain C: Asp108, Asn109		Chain A: Glu161 Chain B: 161 Chain C: Glu161, Asp108
 SYL1655	Anti-HIV Protease inhibitor	Chain A: Val159, Gly160, Leu162 Chain B: Leu162, Cys270, Gly160 Chain C: Cys270, Leu162, Val159	Chain A: Asn109, Thr158, Gln269 Chain B: Asn109, Gln269 Chain C: His89, Gln269			Chain A: Asp108, Glu161 Chain B: Glu161 Chain C: Glu161, Asp108
 Batefenterol	α ₂ adrenoceptors agonist, muscarinic receptor antagonist	Chain A: Val159, Ala86 Chain B: Leu162, Tyr171, Gly160 Chain C: Trp93, Ala107, Val159	Chain A: Thr58, Ser85, His89 Chain B: Asn156, His89	Chain C: Asp108, Chain B: Glu161		Chain A: Glu161, Arg82, Lys157 Chain B: Glu167, Glu161 Chain C: Lys92, Asp108

(continued)

Table 8. Continued.

Compound	Mode of Action	Hydrophobic	Polar	π - π Stacking	H-Bond	Charged
 Camptothecin	Antineoplastic Inhibits RNA Polymerase activity	Chain A: Val159, Leu162, Ala86, Gly160 Chain B: Val159, Cys270 Chain C: Leu162, Cys270, Gly160	Chain A: Thr158, Ser85, His89, Gln269 Chain B: Gln269, His89, Asn109 Chain C: Asn109, Gln269, Thr158	Chain A: Val159		Chain A: Arg82, Glu161 Chain B: Asp108 Chain C: Glu161
 Quarfloxin	Antimalarial Drug Anti-arthritis	Chain A: Leu162, Gly160 Chain B: Leu162, Val159, Cys270, Gly160	Chain A: Asn109, Gln269, Thr158, Chain B: Thr158, Gln269, Asn109 Chain C: Asn109, Gln269	Chain A: Gly160 Chain B: Val159,	Chain A: Gly160 Chain B: Val159	Chain A: Glu161 Chain B: Glu161
 Hydroxychloroquine	Topoisomerase Inhibitor	Chain A: Leu162, Val159 Chain B: Val159, Gly160, Leu162, Cys270 Chain C: Val159, Leu162, Gly160, Cys270	Chain B: Thr158, Gln269, Asn109 Chain A: Gln269, Thr158, Asn109 Chain C: Asn109, Gln269	Chain B: Gly160		Chain B: Glu161, Asp108 Chain A: Arg108 Glu161 Chain C: Glu161, Asp108
 Elvitegravir	Anti-HIV Inhibitor	Chain A: Leu162 Chain B: Leu162, Gly160, Cys270, Val159 Chain C: Leu162, Gly160, Val159	Chain A: Thr158, Asn109, Gln269 Chain B: Thr158, Gln269, Asn109 Chain C: Asn109, Gln269	Chain B: Leu162, Val159		Chain B: Glu161 Chain A: Glu161 Chain C: Asp108

(continued)

Table 8. Continued.

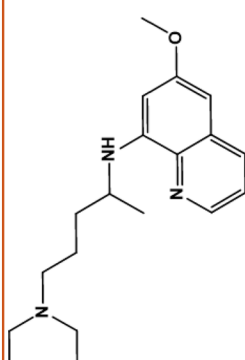
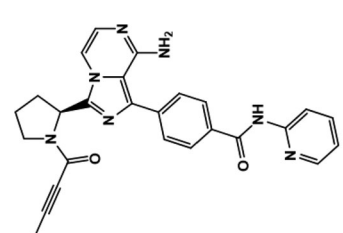
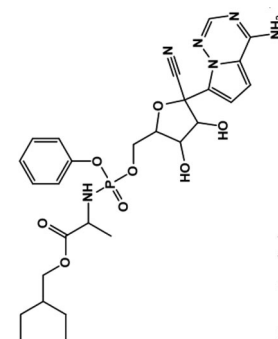
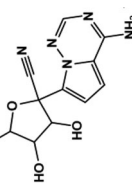
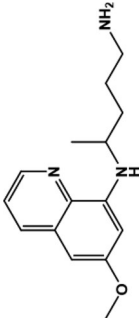
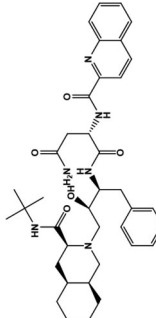
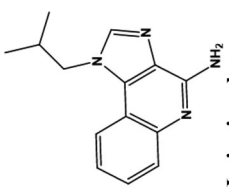
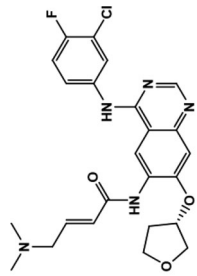

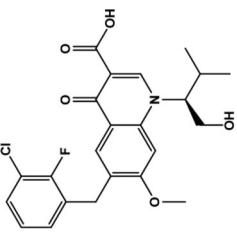
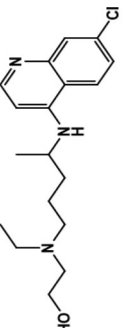
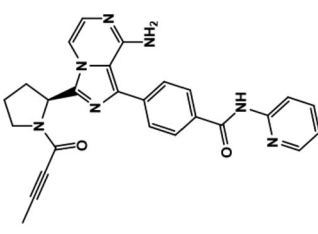
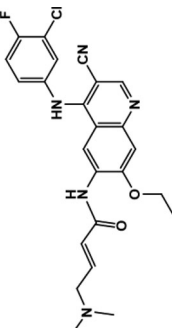
Compound	Mode of Action	Hydrophobic	Polar	π - π Stacking	H-Bond	Charged
	Antimalarial Drug	Chain A: Leu162, Gly160 Chain B: Leu162, Gly160, Cys270, Val159 Chain C: Leu162, Gly160	Chain A: Thr158, Gln269 Chain B: Thr158, Gln269, Asn109, His89 Chain C: Asn109, Gln269	Chain B: Asn109		Chain A: Glu161 Chain B: Asp108 Chain C: Glu161
Plasmoquine 	Tyrosine Kinase inhibitor; Epidermal Growth Factor Receptor (EGFR) inhibitor	Chain A: Leu162, Gly160 Chain B: Leu162, Gly160, Cys270, Chain C: Leu162, Gly160, Ala86, Val159, Cys270	Chain A: Asn109, Gln269 Chain B: Asn109, Gln269 Chain C: Asn109, Gln269, His89, Thr158, Ser85	Chain C: Val159		Chain A: Glu161 Chain B: Glu161 Chain C: Glu161, Asp108
Acalabrutinib 	Antiviral Drug	Chain A: Leu162, Gly160, Val159 Chain B: Leu162, Gly160, Cys270, Val159 Chain C: Leu162, Gly160, Val159, Cys270	Chain A: Asn109, Thr158, Gln269 Chain B: Gln269, Asn109, His89, Thr158 Chain C: Gln269, Asn109, Thr158	Chain C: Asn109 Chain B: Asn109, Gly160		Chain A: Glu161 Chain B: Asp108, Glu161 Chain C: Glu161, Asp108
Remdesivir 						

Table 9. Ligand interaction information for top ranking drug with Nucleocapsid Protein of SARS-COV-2 (PDB ID 6M3M).

Compound	Mode of Action	Hydrophobic	Polar	H-Bond	π-π stacking	Charged
	Antimalarial	Chain A: Ala91, Ala51, Tyr110, Tyr112, Pro118, Chain B: Trp133, Val134, Tyr124, Pro68, Ile132, Phe67, Gly125	Chain A: Asn49, Thr50	Chain B: Trp133	Chain A: Tyr110, Chain B: Lys66	Chain A: Arg108, Arg90, Arg90, Arg93 Chain B: Arg89, Arg69, Lys66
Primaquine	Anti-HIV Protease inhibitor	Chain A: Tyr112, Pro118, Ala51, Tyr110 Chain C: Val159, Tyr173, Trp133, Val134, Tyr124, Ala135, Pro68, Ile132, Phe67, Gly70, Gly125	Chain A: Asn49, Thr50, Ser52 Chain C: Thr55	Chain A: Thr50, Lys66, Chain B: Phe67		Chain A: Arg108, Arg150 Chain B: Arg69, Lys66
	Anti-HIV inhibitor	Chain A: Tyr112, Tyr110, Ala51, Ala91, Pro152, Chain B: Phe67, Pro68, Trp133 Chain C: Val159	Chain A: Ser52, Thr50, Asn49	Chain A: Tyr110, Tyr112, Ser52 Chain B: Arg69	Chain A: Tyr110, Lys66	Chain A: Arg108, Arg93 Chain B: Lys66, Arg69
Saquinavir	Antibacterial	Chain A: Pro118, Ala91, Ala51, Tyr110, Tyr112 Chain B: Pro68, Phe67, Pro169	Chain A: Ser52 Chain B: Thr92 Chain C: Thr167	Chain A: Tyr112 Chain B: Lys66	Chain B: Lys66, Arg89	Chain A: Arg150, Arg108, Arg93 Chain B: Arg89, Lys66
	Tyrosine Kinase inhibitor; Epidermal Growth Factor Receptor (EGFR) inhibitor	Chain A: Tyr110, Ala51, Pro152, Ala157 Chain B: Gly70, Pro68 Chain C: Tyr173, Val159, Leu162, Leu168, Leu160, Leu57	Chain A: Asn49 Chain B: Thr167, Gln71 Chain C: Gln161	Chain B: Arg69		Chain A: Arg150, Arg93, Arg108 Chain B: Arg69, Lys66
Elvitegravir						
						
Imiquimod						
						
Afatinib						

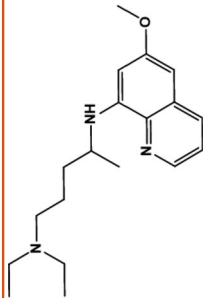
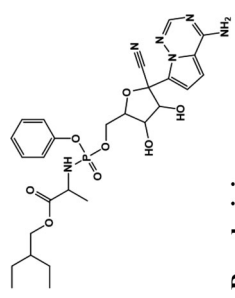
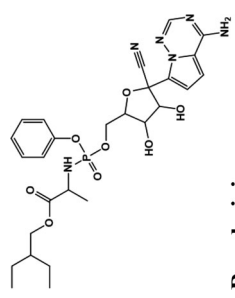
(continued)

Table 9. Continued.

Compound	Mode of Action	Hydrophobic	Polar	H-Bond	π - π stacking	Charged
	Antimalarial	Chain C: Leu160, Leu162, Leu168, Pro163, Gly165, Tyr173, Val159, Leu57 Chain B: Pro163, Gly70, Pro81, Pro68	Chain C: Gln161, Thr166, Gln164, Thr167 Chain B: Thr136, Gln71, Gln164, Gln84, Thr167	Chain C: Gly165, Chain B: Glu137		Chain B: Glu137, Arg69, Chain A: Arg108
Pamaquine						
	Antimalarial Drug Anti-arthritis	Chain B: Pro81, Ile75, Pro74, Val73, Pro163, Gly70 Chain C: Leu168, Pro163, Leu162, Gly165	Chain B: Gln71, Gln164, Gln84, Ser79, Ser80 Chain C: Gln161, Thr166, Gln164, Thr167	Chain C: Leu162		Chain B: Glu137
Hydroxychloroquine						
	Tyrosine Kinase inhibitor; Epidermal Growth Factor Receptor (EGFR) inhibitor	Chain B: Trp133, Tyr124, Pro68, Phe67, Gly125, Leu168, Pro169 Chain A: Tyr112, Ala91, Ala51, Tyr110, Pro152 Chain C: Tyr173	Chain A: Asn49, Thr50, Ser52, Thr92 Chain B: Thr167, Thr50, Ser52	Chain A: Thr50	Chain B: Lys66	Chain A: Arg93, Arg108, Arg94 Chain B: Arg69, Lys66
Acalabrutinib						
	An irreversible Epidermal Receptor Growth receptor Tyrosine kinase	Chain C: Val159, Tyr173, Pro118 Chain A: Tyr112, Ala51 Chain B: Trp133, Val134, Tyr124, Ala135, Pro68, Ile132, Phe67, Gly70	Chain C: Gln161 Chain B: Gln71 Chain A: Asn49, Thr50, Ser52	Chain B: Arg69, Trp133, Phe67	Chain B: Lys66, Gly70, Ala135	Chain B: Arg69, Lys66
EKB-569						

(continued)

Table 9. Continued.

Compound	Mode of Action	Hydrophobic	Polar	H-Bond	π - π stacking	Charged
	Antimalarial Drug	Chain C: Leu162, Pro163, Leu168, Gly165, Chain B: Pro163, Gly70, Pro81, Ile 75	Chain C: Thr167, Thr166, Gln164, Gln161 Chain B: Gln84, Ser79, Asn76, Thr136, Thr77, Gln164, Gln71, Thr166	Chain B: Gly70		Chain B: Glu137
	Antiviral Drug	Chain B: Ala126, Tyr124, Ile131, Ile132, Trp133, Val134, Ala135, Gly125, Gly70, Chain A: Tyr110, Pro152, Ala51 Chain C: Val159	Chain B: Asn127, Gln71, Chain A: Thr50, Asn49	Chain A: Arg150, Thr50, Chain B: Trp133, Lys66		Chain A: Arg150, Lys66 Chain B: Lys128, Arg69
						

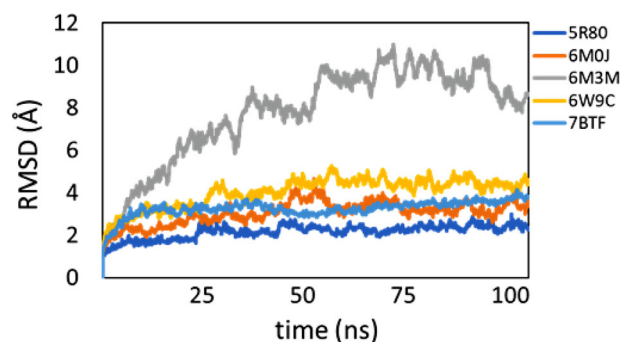


Figure 10. RMSD Plot for all targets of SARS-COV-2 with afatinib drug.

Table 10. Docking parameters of top scorer drugs for nucleocapsid protein of SARS-COV-2 (PDB ID 6M3M).

Drugs	GScore	DScore	Lipophilic EVDW	HBond	EModel
Primaquine	-8.51	-7.58	-2.56	-0.86	-60.692
Amodiaquine	-8.5	-5	-2.6	-0.9	-56.71
Saquinavir	-7.61	-6.65	-4.64	-1	-78.879
Elvitegravir	-7.57	-7.44	-2.76	-1.4	-67.765
Imiquimod	-7.29	-7.03	-2.14	-2.98	-56.262
Afatinib	-7.26	-6.03	-3.29	-0.97	-58.428
Pamaquine	-7.23	-7.23	-5.19	-1.33	-81.96
HQC	-4.99	-4.94	-3.38	-1.28	-40.568
Remdesivir	-6.85	-6.85	-4.64	-1.75	-69.954
Acalabrutinib	-5.15	-5.14	-4.05	-0.92	-72.062
EKB-569	-3.58	-1.76	-3.91	-1.1	-55.435
Plasmaquine	-2.63	-2.4	-4.43	-0.96	-56.61

Absorption: Primaquine, amodiaquine, and HCQ have high Caco-2 (heterogeneous human epithelial colorectal adenocarcinoma cells) permeability.

Human Intestinal Absorption: All drugs are majorly absorbed by human intestine. (For Ideal drug, HIA percentage should be higher than 30%) and primaquine and amodiaquine are highly absorbed by the intestine.

P-Glycoprotein substrate and Inhibitor: P-Glycoprotein is mainly known as multidrug resistance protein; ATP binding cassette subfamily B member is an integral part of cell membrane which flush out foreign substances out of the cell. The results indicate that only primaquine and HCQ are non-inhibitors substrates for P-Glycoprotein.

Distribution: The Distribution results indicate the following observation.

BBB Permeation: For ideal drug Log BBB value, much be greater than 0.3. All drugs are able to cross the Blood-Brain Barrier.

Metabolism:

CY2D6, CY34A: Cytochrome 450 is an enzyme that is encoded by both CY2D6 and CY34A gene, which are primarily expressed and metabolized in the liver. The results indicate that all drugs are except amodiaquine and primaquine are non-inhibitors to CY2D6 substrate and inhibitor and afatinib, acalabrutinib, and primaquine are non-inhibitors to CY34A substrate.

OATP1B1, OATP1B3: OATP1B1 and OAT1B3 are uptake transporters that are expressed on the sinusoidal site of hepatocytes, and these are responsible for drug uptake and endogenous compounds from the blood. The results indicate that all

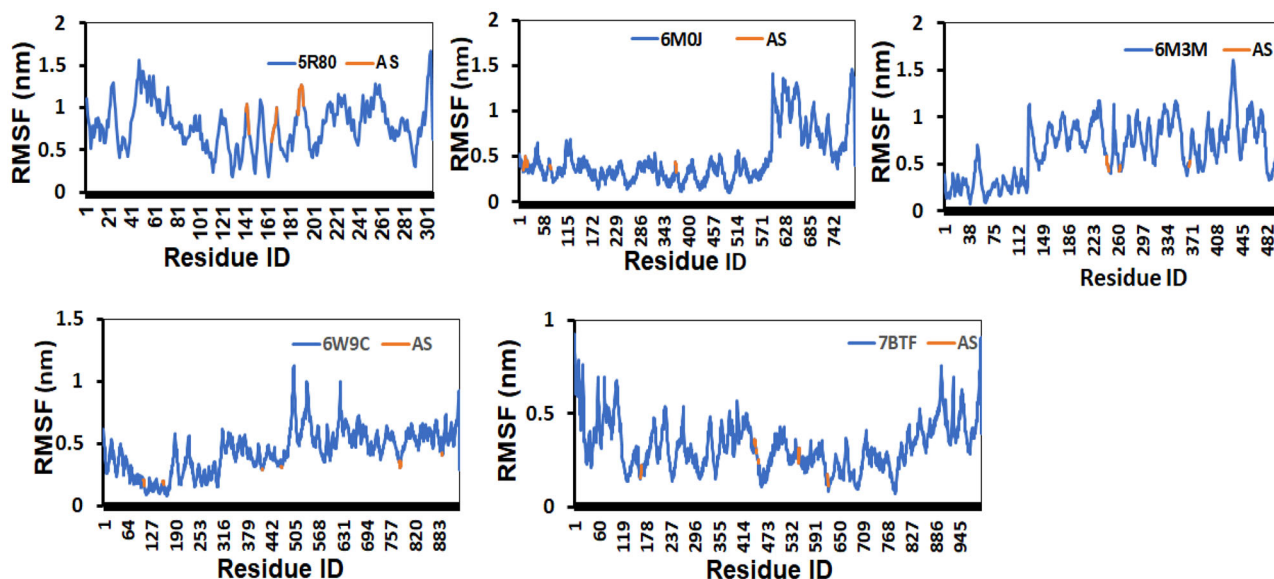


Figure 11. The RMSF fluctuations is shown for the whole complex (blue) and for the active site residues (orange). The RMSF fluctuations with respect to the residue number of the protein-ligand complexes considered for the study is shown in Figure Y. Except 5R80 complex, we observed that the active site residues and the ligand displayed stable RMSF fluctuations. Due to random coil structural elements present in the complexes, which is known to display huge structural fluctuations, we noticed high RMSF fluctuations in these regions. Overall, the stable RMSF profile suggests that the protein-ligand complexes are stable during the course of simulations.

Table 11. Docking Parameters of Top scoring Drugs to target RNA dependent RNA Polymerase from SARS-COV-2 (PDB ID 7BTF).

Drugs	GScore	DScore	Lipophilic EVDW	HBond	EModel
EKB-569	-8.97	-6.45	-4.4	-2.1	-87.789
Camptothecin	-7.81	-7.1	-6.5	-0.4	-72.146
Amodiaquine	-7.53	-7.53	-5.3	-1.6	-78.285
Primaquine	-7.1	-7	-6.2	-2.5	-71.433
Dequalinium	-7.04	-6.4	-5.2	-0.7	-78.145
Elvitegravir	-7.04	-4.19	-1.92	-1.78	-80.599
Imiquimod	-6.7	-6.6	-4	-1.9	-59.016
Saquinavir	-6.4	-6.4	-5.8	-2	-87.479
Afatinib	-5.9	-4	-5.2	-0.5	-73.441
Acalabrutinib	-5.4	-5	-4.3	-0.7	-73.387
Hydroxychloroquine	-6.1	-5.11	-4.4	-1.2	-44.626
Remdesivir	-8.4	-8.4	-5.6	-2.3	-82.944
Galidesivir	-5.4	-5.3	-0.7	-3.3	-42.332

quinoline drugs except afatinib is non-inhibitor for OATP1B1. All drugs are inhibitors of OATP1B1 and OATP1B3, which led to the conclusion that drugs may be metabolized by the liver.

Excretion:

OCT2, MATE-1 Inhibitor:

All quinoline based drugs except primaquine are non-inhibitor to Organic cation Transporter 2 (OCT2) and Multidrug and toxic extrusion (MATE-1) inhibitor which concluded that all drugs are eliminated from urine.

Toxicity:

The toxic analysis indicates that all quinoline drugs are non-carcinogenic and non-toxic.

Hence all ADME results indicate that best scorer quinoline drugs have ideal properties to work as anti-SARS-COV-2 therapeutic drugs.

3.4. Enrichment studies

Enrichment studies help to assess the active set of compounds statically among large set of databases through virtual screening. The parameters that are calculated through enrichment

studies are Receiver Operator Characteristics area under the curve (ROC), Boltzmann-enhanced Discrimination Receiver Operator Characteristic area under the curve and Enrichment Factor (BERDOC), and Enrichment factor calculated with respect to the number of total ligands. $EF = (a/n)/(A/N)$, where a is the number of actives found in sample size n , A is the total number of actives, and N is the total number of ligands (decoys and actives). All these parameters are summarized in the Table 13.

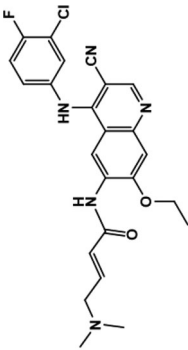
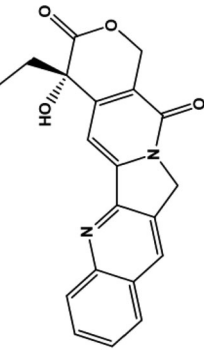
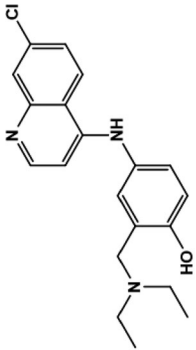
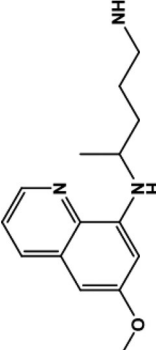
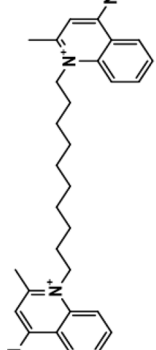
The ideal value for BERDOC and ROC parameters should be between 0 and 1. The active ligands among whole databases and decoys with all five targets main protease, spike proteins, RdRp enzymes, papain protease as well as for N protein of SARS-CO-2 have value below 1 which indicates that the active ligands are ideal to work against therapeutic targets of SARS-COV-2. The ROC curves for active ligands with each target are shown in Figure 9.

3.5. Molecular dynamics simulation

The protein-Afatinib complexes: afatinib-5R80, afatinib-6M0J, afatinib-6W9C, and afatinib-7BTF showed very stable RMSD fluctuations ($< 3.6 \text{ \AA}$) throughout the simulation's trajectories. Among the four stable complexes, 7BTF and 5R80 had the least variation in the backbone. Afatinib-6M3M complex displayed dramatic RMSD fluctuations (2-8.25 Å with spikes upto 11 Å) during the course of simulations. On visualizing the MD simulation trajectories, it was observed that the high RMSD fluctuations in 6M3M are due to the movement of one of the protein subunits in the protein, though the ligand remained in the active site of the protein. The RMSD fluctuations are shown in Figure 10.

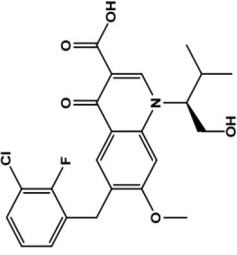
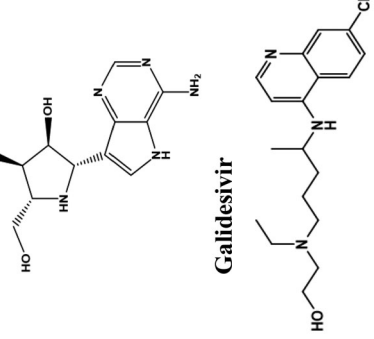
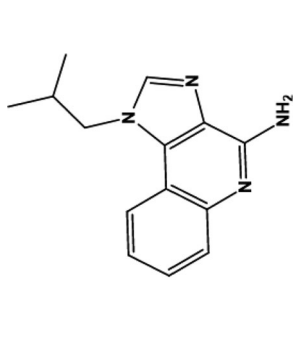
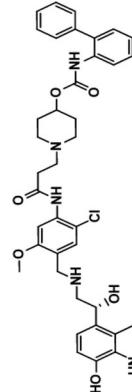
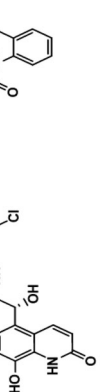
The RMSF fluctuations with respect to the residue number of the protein-ligand (Afatinib) complexes considered for the study is shown in Figure 11. Except for the afatinib-6M0J

Table 12. Interacting amino acids for compounds having G-Score above Hydroxyquinoline and Galidesivir for RNA dependent RNA Polymerase of SARS-COV-2 (PDB ID 7BTF).

Compound	Mode of Action	Hydrophobic	Polar	H-Bond	π-π stacking	Charged
 EKB-569	Potent Irreversible EGFR receptor	Tyr455, Ala554, Val557, Tyr619, Pro620, Cys622	Thr556, Ser682, Ser759	Asp760, Asp760, Arg553, Arg553, Asp623, Asp623, Asp623	Lys621, Arg553, Arg553, Arg553	Lys621, Arg553, Arg624, Arg555, Arg545, Asp452, Asp623, Asp760, Asp761
 Camptothecin	DNA Topoisomerase inhibitor	Tyr455, Tyr619, Pro620, Cys622, Ala550	Ser549	Asp760, Asp760, Asp623, Lys621, Tyr619	Lys621, Arg553, Arg553	Lys798, Arg621, Arg624, Arg555, Arg553, Lys551, Asp623, Asp618, Asp761, Asp760
 Amodiaquine	Antimalarial, Anti-inflammatory	Tyr455, Cys622, Pro620, Tyr619, Trp617, Ala762	Trp617, Trp617, Asp761, Asp760, Lys621, Asp761	Asp761, Trp617, Asp760, Lys621, Asp761	Arg553, Lys621	Lys551, Arg553, Arg555, Arg624, Lys621, Lys798, Asp623, Asp618, Asp761, Asp760
 Primaquine	Antimalarial	Tyr455, Cys622, Pro620, Tyr619, Trp617, Ala762	Ser759	Asp760, Asp760, Asp761	Lys621, Arg553, Arg553, Asp452	Lys551, Arg553, Asp452, Arg624, Asp623, Lys621, Asp618, Asp760, Asp761, Lys798
 Dequalinium	Antibiotic	Tyr455, Ala554, Cys622, Pro620, Tyr619, Trp617, Ala762, Trp800, Phe812, Cys814	Thr556, Ser682, Ser814	Asp452, Asp623, Asp761, Trp617	Arg553, Arg553	Arg553, Arg555, Arg624, Lys621, Lys798, Asp452, Asp623, Asp618, Asp761, Asp760, Glu811

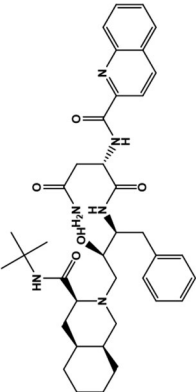
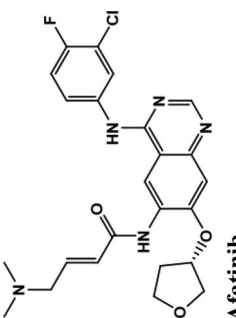
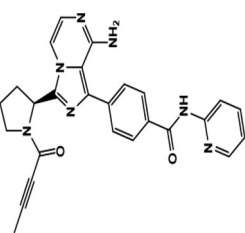
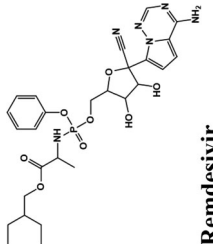
(continued)

Table 12. Continued.

Compound	Mode of Action	Hydrophobic	Polar	H-Bond	π - π stacking	Charged
	Anti-HIV inhibitor	Tyr619, Pro620, Cys622, Tyr455,	Asn691, Thr680, Ser682, Thr556	Arg553, Asn691, Arg555	Lys621, Arg553	Asp618, Asp760, Asp623, Lys621, Arg624, Arg553, Arg555,
Elvitegravir	Antiviral activity against positive and negative sense RNA viruses for example: Ebola, Marburg, Yellow fever, Zika virus	Tyr619, Pro620, Cys622, Tyr455	Thr556	Asp623, Asp618, Tyr619		Asp618, Asp760, Asp623, Asp452, Lys798, Lys621, Arg624, Arg553, Lys551
	Antimalarial Drug Anti-arthritis	Cys622, Pro620, Tyr619, Trp617, Trp800, Ala762, Phe812, Cys813	Ser814	Asp760, Asp761, Asp761, Asp623	Lys621	Asp623, Lys621, Asp618, Asp760, Asp761, Glu811, Lys798
Galidesivir						
	Toll-like receptor 7 Agonist	Tyr619, Pro620, Cys622, Tyr455		Asp623, Arg553, Arg555	Lys621, Arg553	Lys621, Asp623, Asp618, Lys798, Arg624, Asp760, Asp452
Hydroxychloroquine						
	β_2 adrenoceptors agonist, muscarinic receptor antagonist	Cys622, Pro620, Tyr619, Trp617, Tyr455, Ala554	Ser759, Asn691, Thr556, Ser814	Lys621, Asp618, Asp760, Ala554	Lys621, Tyr455, Arg553	Lys621, Arg624, Asp623, Asp618, Lys551, Arg553, Arg555, Asp760, Asp761
Imiquimod						
						
Batefenterol						

(continued)

Table 12. Continued.

Compound	Mode of Action	Hydrophobic	Polar	H-Bond	π - π stacking	Charged
	Anti-HIV Protease Inhibitor	Tyr619, Trp617, Pro620, Cys622, Ala762, Ala688	Ser682, Thr687, Asn691, Thr556, Ser759	Asp760, Asp623, Arg553, Arg555, Thr556		Asp618, Glu811, Lys621, Arg624, Asp623, Lys545, Asp684, Arg555, Arg553, Asp760, Asp761
Saquinavir						
	Tyrosine Kinase inhibitor; Epidermal Growth Factor Receptor (EGFR) inhibitor	Chain A: Tyr455, Ala554, Ala448	Chain A: Asn552, Ser451, Asn447, Gln444 Chain C: Gln34	Chain A: Ala554, Asp445	Chain A: Arg553, Ala554	Chain A: Lys621, Arg624, Lys551, Arg553, Asp623, Asp445
Afatinib						
	Tyrosine Kinase inhibitor; Epidermal Growth Factor Receptor (EGFR) inhibitor	Pro620, Cys622, Val166, Tyr455, Ala688	Ser759, Asn691, Thr680, Ser681, Ser682	Asp623, Lys621	Arg553	Lys798, Glu167, Asp760, Asp623, Arg624, Lys621, Arg553, Lys551
Acalabrutinib						
	Antiviral Drug	Tyr619, Val166, Pro620, Cys622, Met626, Tyr455	Ser759, Thr680, Asn691, Asn552	Lys798, Lys621, Cys622	Arg553, Lys621	Asp618, Lys798, Lys621, Arg624, Asp623, Lys551, Arg553, Asp760
Remdesivir						

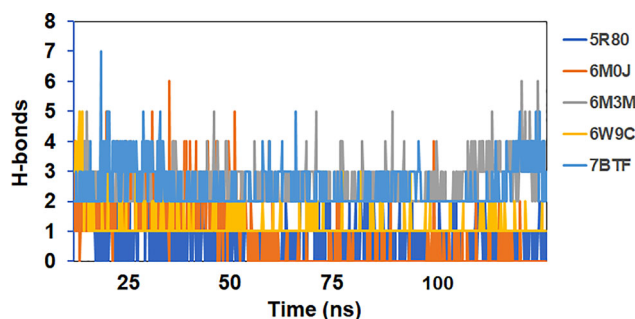


Figure 12. Number of H-bonds vs. run-length for all the complexes considered for the study.

Table 13. Enrichment Parameters for all therapeutics targets of SARS-COV-2.

Parameters	6M0J	5R80	6W9C	7BTF	6M3M
BERDOC	0.234	0.363	0.335	0.216	0.320
ROC	0.76	0.78	0.76	0.62	0.55
EF	20%	40%	40%	30%	30%

Table 14. MM-PBSA Energy calculation.

S. No	PDB	Binding Free Energy
1	5R80	-5.44 ± 0.69 kcal/mol
2	6M0J	-4.29 ± 0.38 kcal/mol
3	6M3M	-7.66 ± 0.54 kcal/mol
4	6W9C	-4.16 ± 0.44 kcal/mol
5	7BTF	-11.19 ± 0.72 kcal/mol

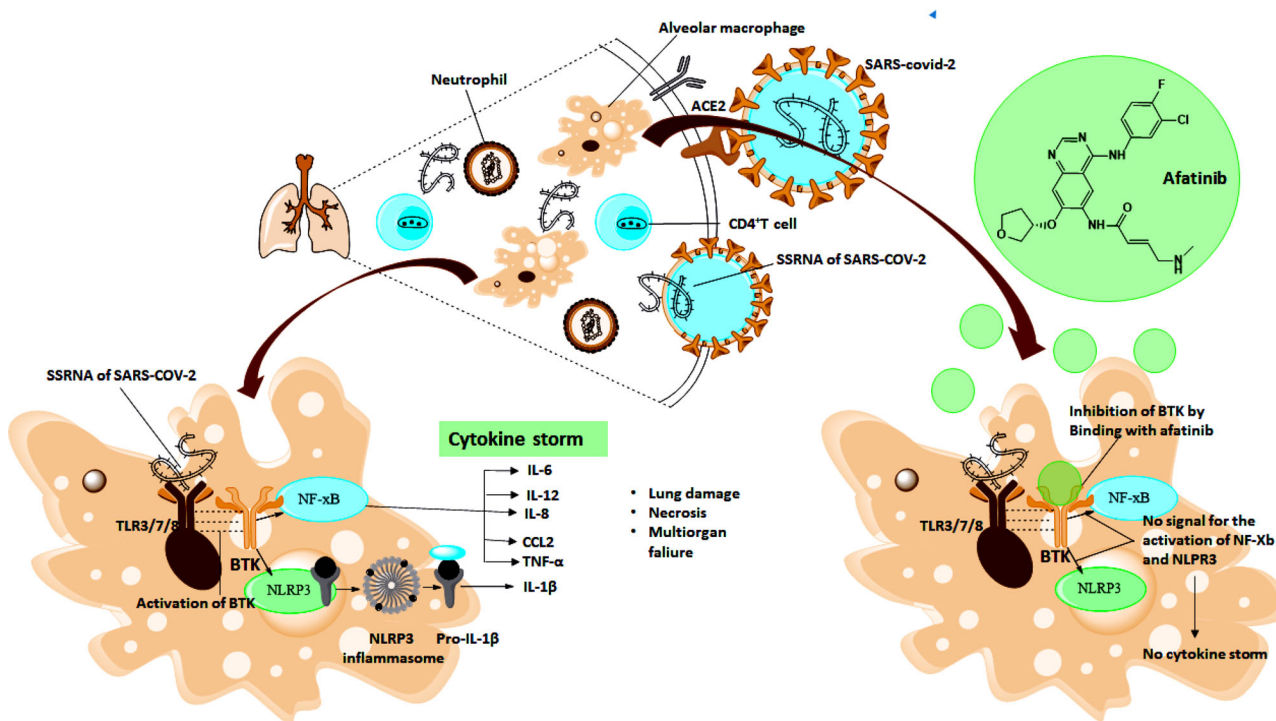


Figure 13. SSRNA of SARS-COV-2 binds with toll like receptors (in macrophages) which activates the Bruton Tyrosine Kinase (BTK), triggering the production of various inflammatory cytokines (cytokine storm). Afatinib act as BTK Inhibitor and inhibit the activation of cytokine storm.

complex, it was observed that the active site residues and the ligand displayed RMSF fluctuations. Due to random coil structural elements present in the complexes, which are known to display huge structural fluctuations, we noticed high RMSF fluctuations in these regions. Overall, the stable RMSF profile suggests that the protein-ligand complexes are stable during the course of simulations.

The average number of hydrogen bonds in protein-ligand (Afatinib) complexes 5R80, 6M0J, 6M3M, 6W9C, and 7BTF were 1, 1, 2, 1, and 3, respectively. Thus, the maximum number of hydrogen bond interactions were shown by ligand in complexation with (RdRp) RNA dependent RNA polymerase enzyme of SARS-COV-2 while maintaining several van-der Waals contacts. The number of H-bonds formed in the protein-ligand complexes considered for the study as a function of run-length is shown in Figure 12.

3.6. MM-PBSA calculation

MM-PBSA calculation provide overview about the molecular interaction and free binding energy of Afatinib-protein

complex. We computed the Binding free energies of the ligand to the protein via MM-PBSA calculations. We also utilized the last 20 ns of the simulations trajectories and generated 80 frames for processing the data for binding energy calculations. The observed binding free energies were: 5R80 (-5.44 ± 0.69 kcal/mol), 6M0J (-4.29 ± 0.38 kcal/mol), 6M3M (-7.66 ± 0.54 kcal/mol), 6W9C (-4.16 ± 0.44 kcal/mol), and 7BTF (-11.19 ± 0.72 kcal/mol). The high binding free energy of the complex with RNA dependent RNA polymerase (7BTF) from SARS-COV-2 suggested (Table 14) that the afatinib could be helpful most in inhibiting the replication process of single stranded RNA virus.

3.6.1. Biological Mechanism by which Afatinib inhibit the activity of SARS-COV-2 (Figure 13)

Afatinib belongs to the tyrosine kinase inhibitor family of medication. It is also used to treat non-small lung cell carcinoma, which maintains mutation in the Epidermal Growth factor receptor in a gene (Roskoski, 2016). SARS-Cov-2 virus, when

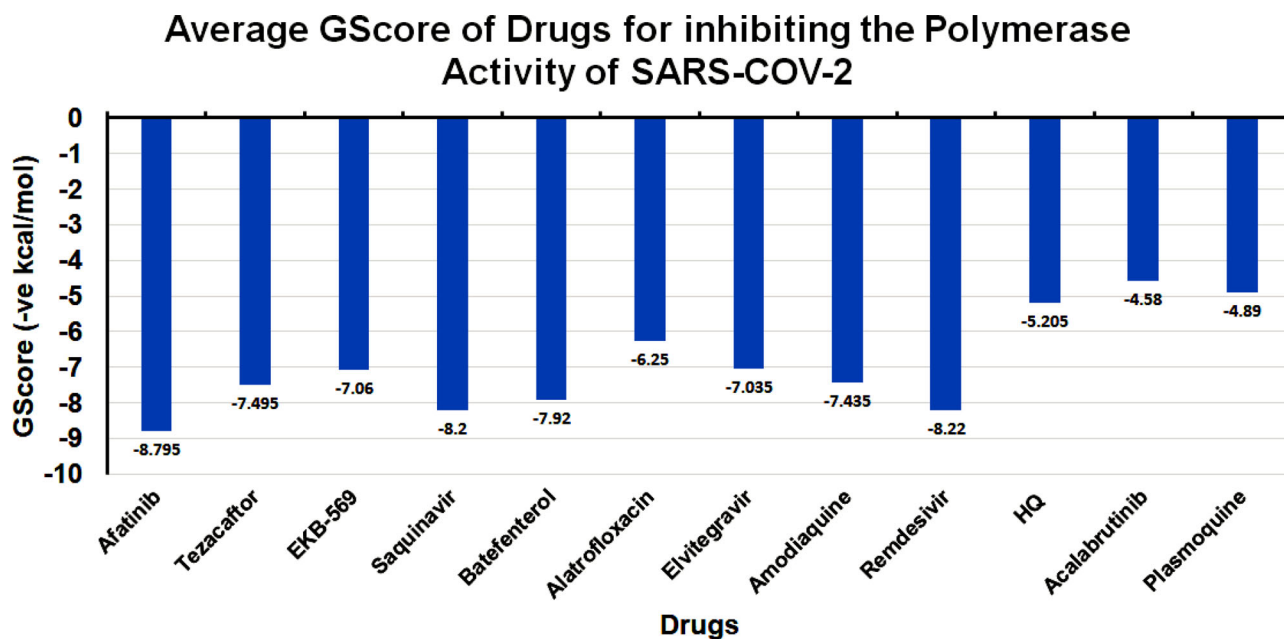


Figure 14. Average GScore of top-ranking Drugs for Protease (Main and Papain) to inhibit the activity of SARS-COV-2.

entered into the body simultaneously, binds with ACE-2 and TMPRSS-2 receptor through which it penetrates the lungs where it releases its single-stranded RNA virus to start multiplication to form multiple copies of a single-stranded virus. During this multiplication process, RNA of COV-2 binds with Toll-like receptors present in the macrophages, further activating the Bruton Tyrosine Kinase. Bruton Kinase Inhibitor plays an essential role in patients suffering from the coronavirus due to macrophage activation (Roschewski et al., 2020). BTK deals with macrophage signalling and activation, which leads to the hyperinflammatory immune response in corona patients. After activation, BTK sends signals to NF- κ B, which triggers various inflammatory cytokines (IL-6, IL-12, IL-8, CCL2, TNF- α). BTK also activates the NLRP3 inflammasome to secrete the IL1 β . A virus-induced hyperinflammatory response or “cytokine storm” may be an important pathogenic mechanism of ARDS in these patients by altering pulmonary macrophages and neutrophils, which can lead to the death of patients (Figure 13).

Hence BTK plays a vital role in the activation of these inflammatory cytokines (Conti et al., 2020). BTK inhibitors can inhibit the activity of BTK signalling from macrophage to other inflammatory Cytokines. Afatinib is a potent Bruton tyrosine kinase inhibitor drug (de Bruin et al., 2020). Afatinib breaks the chain of signalling from macrophages activation to auto-immune cells (IL-6, IL-12, IL-8, CCL2, TNF- α) (de Bruin et al., 2020). Therefore, it inhibits the process of activation and cytokine storm. Afatinib also supports human innate immune system response, thereby helping in controlling in replication and infection of virus therefore expected to enhance the immune response (Roschewski et al., 2020).

4. Conclusion

This study showed that among tested drugs in the present in silico study, Afatinib has the highest binding potential to the main protease of SARS-CoV-2, which is higher than HCQ

and remdesivir, respectively. (Figure 14) Likewise, other drugs amodiaquine, saquinavir showed efficient binding with active sites on the main protease, papain protease, and RdRp. Among all the screened drugs, Afatinib serves as the best candidate inhibitor for binding with (a) main protease M^{Pro} of SARS-COV-2 with a GScore of -9.04 kcal/mol. Docking with 7BTF RdRp suggests that EKB-569 has the highest binding with GScore value -8.97 kcal/mol. Docking with papain-like protease PL^{Pro}, (PDB ID 6W9C) amodiaquine and Afatinib are active binders with GScore -8.57 kcal/mol and -8.53 kcal/mol, respectively. Docking with Nucleocapsid proteins of SARS-COV-2 suggests that primaquine and amodiaquine serve as the best inhibitor with GScore -8.51 kcal/mol and remdesivir used as control have GScore -6.8 kcal/mol. From docking analysis, it is concluded that Afatinib, amodiaquine, saquinavir, and primaquine are the best drugs to inhibit the entry replication and transcription of viral genome of SARS-COV-2. Further, as we screened Afatinib could be best candidate to overall inhibit the process of SARS-COV-2. Molecular dynamics simulations of Afatinib drug with each therapeutics target of SARS-COV-2, followed by binding free energy estimations via MM-PBSA methods, suggested that the Afatinib-7BTF complex is the most stable complex with the highest ligand binding energetics.

Acknowledgements

The authors would like to thank Department of Chemistry, University of Delhi, New Delhi, India and Institute of Nuclear Medicine and Allied Sciences, Défense Research Development Organization, New Delhi, India for providing Schrodinger Software and other facilities to accomplish this work. The authors also would like to thank UGC for providing fellowship. The authors one and two have equal contribution.

Disclosure statement

The authors declare no conflict of interest.

ORCID

Anju Anju  <http://orcid.org/0000-0002-0709-3137>
 Shubhra Chaturvedi  <http://orcid.org/0000-0003-0285-2111>
 Vishakha Chaudhary  <http://orcid.org/0000-0002-9589-3846>
 Pradeep Pant  <http://orcid.org/0000-0003-3890-1958>
 Firasat  <http://orcid.org/0000-0003-0639-7638>
 Anil Kumar Mishra  <http://orcid.org/0000-0002-7467-9146>

References

- Alexpandi, R., De Mesquita, J. F., Pandian, S. K., & Ravi, A. V. (2020). Quinolines-Based SARS-CoV-2 3CLpro and RdRp Inhibitors and Spike-RBD-ACE2 Inhibitor for Drug-Repurposing Against COVID-19: An in silico Analysis. *Frontiers in Microbiology*, 11(July), 1796–1715. <https://doi.org/10.3389/fmicb.2020.01796>
- Barnard, R. A., Wittenburg, L. A., Amaravadi, R. K., Gustafson, D. L., Thorburn, A., & Thamm, D. H. (2014). Phase I clinical trial and pharmacodynamic evaluation of combination hydroxychloroquine and doxorubicin treatment in pet dogs treated for spontaneously occurring lymphoma. *Autophagy*, 10(8), 1415–1425. <https://doi.org/10.4161/autophagy.29165>
- Bhardwaj, V. K., Singh, R., Sharma, J., Rajendran, V., Purohit, R., & Kumar, S. (2020). Identification of bioactive molecules from tea plant as SARS-CoV-2 main protease inhibitors. *Journal of Biomolecular Structure and Dynamics*, 1–10. <https://doi.org/10.1080/07391102.2020.1766572>
- Braga, S. F. P., Martins, L. C., da Silva, E. B., Sales Júnior, P. A., Murta, S. M. F., Romanha, A. J., Soh, W. T., Brandstetter, H., Ferreira, R. S., & de Oliveira, R. B. (2017). Synthesis and biological evaluation of potential inhibitors of the cysteine proteases cruzain and rhodesain designed by molecular simplification. *Bioorganic & Medicinal Chemistry*, 25(6), 1889–1900. <https://doi.org/10.1016/j.bmc.2017.02.009>
- Cao, B., Wang, Y., Wen, D., Liu, W., Wang, J., Fan, G., Ruan, L., Song, B., Cai, Y., Wei, M., Li, X., Xia, J., Chen, N., Xiang, J., Yu, T., Bai, T., Xie, X., Zhang, L., Li, C., ... Wang, C. (2020). A trial of lopinavir-ritonavir in adults hospitalized with severe covid-19. *The New England Journal of Medicine*, 382(19), 1787–1799. <https://doi.org/10.1056/NEJMoa2001282>
- Chakraborty, H., & Bhattacharjya, S. (2020). Mechanistic insights of host cell fusion of SARS-CoV-1 and SARS-CoV-2 from atomic resolution structure and membrane dynamics. *Biophysical Chemistry*, 265(June), 106438. <https://doi.org/10.1016/j.bpc.2020.106438>
- Chakraborty, C., Sharma, A. R., Bhattacharya, M., Sharma, G., Lee, S. S., & Agoramoorthy, G. (2020). COVID-19: Consider IL-6 receptor antagonist for the therapy of cytokine storm syndrome in SARS-CoV-2 infected patients. *Journal of Medical Virology*, 92(11), 2260–2263. <https://doi.org/10.1002/jmv.26078>
- Cheatham, T. E. I. I., Miller, J. L., Fox, T., Darden, T. A., & Kollman, P. A. (1995). Molecular dynamics simulations on solvated biomolecular systems: The particle mesh Ewald method leads to stable trajectories of DNA, RNA, and proteins. *Journal of the American Chemical Society*, 117(14), 4193–4194. <https://doi.org/10.1021/ja00119a045>
- Chu, C. M., Cheng, V. C. C., Hung, I. F. N., Wong, M. M. L., Chan, K. H., Chan, K. S., Kao, R. Y. T., Poon, L. L. M., Wong, C. L. P., Guan, Y., Peiris, J. S. M., & Yuen, K. Y. (2004). Role of lopinavir/ritonavir in the treatment of SARS: Initial virological and clinical findings. *Thorax*, 59(3), 252–256. <https://doi.org/10.1136/thorax.2003.012658>
- Conti, P., Ronconi, G., Caraffa, A., Gallenga, C. E., Ross, R., Frydas, I., & Kritas, S. K. (2020). Induction of pro-inflammatory cytokines (IL-1 and IL-6) and lung inflammation by Coronavirus-19 (COVI-19 or SARS-CoV-2): Anti-inflammatory strategies. *Journal of Biological Regulators and Homeostatic Agents*, 34(2), 327–331. <https://doi.org/10.23812/CONTI-E>
- Dai, W., Zhang, B., Jiang, X.-M., Su, H., Li, J., Zhao, Y., Xie, X., Jin, Z., Peng, J., Liu, F., Li, C., Li, Y., Bai, F., Wang, H., Cheng, X., Cen, X., Hu, S., Yang, X., Wang, J., ... Liu, H. (2020). Structure-based design of antiviral drug candidates targeting the SARS-CoV-2 main protease. *Science (New York, N.Y.)*, 368(6497), 1331–1335. <https://doi.org/10.1126/science.abb4489>
- de Bruin, G., Demont, D., de Zwart, E., Verkaik, S., Hoogenboom, N., van de Kar, B., van Lith, B., Emmelot-van Hoek, M., Gulrajani, M., Covey, T., Kaptein, A., & Barf, T. (2020). Discovery of quinoline-based irreversible BTK inhibitors. *Bioorganic & Medicinal Chemistry Letters*, 30(14), 127261. <https://doi.org/10.1016/j.bmcl.2020.127261>
- Desai, N. C., Patel, B. Y., Jadeja, K. A., Dave, B. P., & Desai, N. C. (2017). Nov appro drug des dev landscapng of quinoline based heterocycles as potential antimicrobial agents: A mini review. *Mini Review*, 1(4), 1–4. <https://doi.org/10.19080/NAPDD.2017.01.555570>
- Dror, R. O., Dirks, R. M., Grossman, J. P., Xu, H., & Shaw, D. E. (2012). Biomolecular Simulation: A Computational Microscope for Molecular Biology. *Annual Review of Biophysics*, 41(1), 429–452. <https://doi.org/10.1146/annurev-biophys-042910-155245>
- Duan, L., Guo, X., Cong, Y., Feng, G., Li, Y., & Zhang, J. Z. H. (2019). Accelerated Molecular Dynamics Simulation for Helical Proteins Folding in Explicit Water. *Frontiers in Chemistry*, 7(August), 540–518. <https://doi.org/10.3389/fchem.2019.00540>
- Dutta, N. K., Mazumdar, K., & Gordy, J. T. (2020). The Nucleocapsid Protein of SARS-CoV-2: A Target for Vaccine Development. *Journal of Virology*, 94(13), 1–2. <https://doi.org/10.1128/JVI.00647-20>
- Elfiky, A. A. (2020). SARS-CoV-2 RNA dependent RNA polymerase (RdRp) targeting: An in silico perspective. *Journal of Biomolecular Structure and Dynamics*, 1–9. <https://doi.org/10.1080/07391102.2020.1761882>
- Elzupir, A. O. (2020). Inhibition of SARS-CoV-2 main protease 3CLpro by means of α -ketoamide and pyridone-containing pharmaceuticals using in silico molecular docking. *Journal of Molecular Structure*, 1222, 128878. <https://doi.org/10.1016/j.molstruc.2020.128878>
- Hollingsworth, S. A., & Dror, R. O. (2018). Molecular dynamics simulation for all. *Neuron*, 99(6), 1129–1143. <https://doi.org/10.1016/j.neuron.2018.08.011>
- Huang, C., Wang, Y., Li, X., Ren, L., Zhao, J., Hu, Y., Zhang, L., Fan, G., Xu, J., Gu, X., Cheng, Z., Yu, T., Xia, J., Wei, Y., Wu, W., Xie, X., Yin, W., Li, H., Liu, M., ... Cao, B. (2020). Clinical features of patients infected with 2019 novel coronavirus in Wuhan, China. *The Lancet*, 395(10223), 497–506. [https://doi.org/10.1016/S0140-6736\(20\)30183-5](https://doi.org/10.1016/S0140-6736(20)30183-5)
- Joung, I. S., & Cheatham, T. E. (2008). Determination of Alkali and Halide Monovalent Ion Parameters for Use in Explicitly Solvated Biomolecular Simulations. *The Journal of Physical Chemistry B*, 112(30), 9020–9041. <https://doi.org/10.1021/jp8001614>
- Kang, S., Yang, M., Hong, Z., Zhang, L., Huang, Z., Chen, X., He, S., Zhou, Z., Zhou, Z., Chen, Q., Yan, Y., Zhang, C., Shan, H., & Chen, S. (2020). Crystal structure of SARS-CoV-2 nucleocapsid protein RNA binding domain reveals potential unique drug targeting sites. *Acta Pharmaceutica Sinica B*, 10(7), 1228–1238. <https://doi.org/10.1016/j.apsb.2020.04.009>
- Khan, R. J., Jha, R. K., Amera, G. M., Jain, M., Singh, E., Pathak, A., Singh, R. P., Muthukumar, J., & Singh, A. K. (2020). Targeting SARS-CoV-2: A systematic drug repurposing approach to identify promising inhibitors against 3C-like proteinase and 2'-O-ribose methyltransferase. *Journal of Biomolecular Structure and Dynamics*, 39(8), 2679–2692. <https://doi.org/10.1080/07391102.2020.1753577>
- Kiplin Guy, R., DiPaola, R. S., Romanelli, F., & Dutch, R. E. (2020). Rapid repurposing of drugs for COVID-19. *Science (New York, N.Y.)*, 368(6493), 829–830. <https://doi.org/10.1126/science.abb9332>
- Ko, W.-C., Rolain, J.-M., Lee, N.-Y., Chen, P.-L., Huang, C.-T., Lee, P.-I., & Hsueh, P.-R. (2020). Arguments in favour of remdesivir for treating SARS-CoV-2 infections. In *International Journal of Antimicrobial Agents*, 55(4), 105933. <https://doi.org/10.1016/j.ijantimicag.2020.105933>
- Lan, J., Ge, J., Yu, J., Shan, S., Zhou, H., Fan, S., Zhang, Q., Shi, X., Wang, Q., Zhang, L., & Wang, X. (2020). Structure of the SARS-CoV-2 spike receptor-binding domain bound to the ACE2 receptor. *Nature*, 581(7807), 215–220. <https://doi.org/10.1038/s41586-020-2180-5>
- Laskowski, R. A., & Swindells, M. B. (2011). LigPlot+: Multiple ligand-protein interaction diagrams for drug discovery. *Journal of Chemical Information and Modeling*, 51(10), 2778–2786. <https://doi.org/10.1021/ci200227u>
- Law, P. K. (2020). COVID-19 Pandemic: Its Origin, Implications and Treatments. *Open Journal of Regenerative Medicine*, 09(02), 43–64. <https://doi.org/10.4236/ojrm.2020.92006>
- Liu, J., Cao, R., Xu, M., Wang, X., Zhang, H., Hu, H., Li, Y., Hu, Z., Zhong, W., & Wang, M. (2020). Hydroxychloroquine, a less toxic derivative of

- chloroquine, is effective in inhibiting SARS-CoV-2 infection in vitro. In *Cell Discovery*. <https://doi.org/10.1038/s41421-020-0156-0>
- Maier, J. A., Martinez, C., Kasavajhala, K., Wickstrom, L., Hauser, K. E., & Simmerling, C. (2015). ff14SB: Improving the accuracy of protein side chain and backbone parameters from ff99SB. *Journal of Chemical Theory and Computation*, 11(8), 3696–3713. <https://doi.org/10.1021/acs.jctc.5b00255>
- Marella, A., Tanwar, O. P., Saha, R., Ali, M. R., Srivastava, S., Akhter, M., Shaquiquzzaman, M., & Alam, M. M. (2013). Quinoline: A versatile heterocyclic. *Saudi Pharmaceutical Journal : SPJ : The Official Publication of the Saudi Pharmaceutical Society*, 21(1), 1–12. <https://doi.org/10.1016/j.jsps.2012.03.002>
- Onufriev, A., Bashford, D., & Case, D. A. (2000). Modification of the generalized born model suitable for macromolecules. *The Journal of Physical Chemistry B*, 104(15), 3712–3720. <https://doi.org/10.1021/jp994072s>
- Ramser, B., Kokot, A., Metze, D., Weiss, N., Luger, T. A., & Böhm, M. (2009). Hydroxychloroquine modulates metabolic activity and proliferation and induces autophagic cell death of human dermal fibroblasts. *The Journal of Investigative Dermatology*, 129(10), 2419–2426. <https://doi.org/10.1038/jid.2009.80>
- Roe, D. R., & Cheatham, T. E. (2013). PTRAJ and CPPTRAJ: Software for processing and analysis of molecular dynamics trajectory data. *Journal of Chemical Theory and Computation*, 9(7), 3084–3095. <https://doi.org/10.1021/ct400341p>
- Roschewski, M., Lionakis, M. S., Sharman, J. P., Roswarski, J., Goy, A., Monticelli, M. A., Roshon, M., Wrzesinski, S. H., Desai, J. V., Zarakas, M. A., Collen, J., Rose, K., Hamdy, A., Izumi, R., Wright, G. W., Chung, K. K., Baselga, J., Staudt, L. M., & Wilson, W. H. (2020). Inhibition of Bruton tyrosine kinase in patients with severe COVID-19. *Science Immunology*, 5(48), eabd0110. <https://doi.org/10.1126/sciimmunol.abd0110>
- Roskoski, R. (2016). Ibrutinib inhibition of Bruton protein-tyrosine kinase (BTK) in the treatment of B cell neoplasms. *Pharmacological Research*, 113(Pt A), 395–408. <https://doi.org/10.1016/j.phrs.2016.09.011>
- Rothan, H. A., & Byrareddy, S. N. (2020). The epidemiology and pathogenesis of coronavirus disease (COVID-19) outbreak. *Journal of Autoimmunity*, 109, 102433. <https://doi.org/10.1016/j.jaut.2020.102433>
- Sachdeva, C., Wadhwa, A., Kumari, A., Hussain, F., Jha, P., & Kaushik, N. K. (2020). In silico Potential of Approved Antimalarial Drugs for Repurposing Against COVID-19. *OMICS: A Journal of Integrative Biology*, 24(10), 568–580. <https://doi.org/10.1089/omi.2020.0071>
- Santhanam, V., Pant, P., Jayaram, B., & Ramesh, N. G. (2019). Design, synthesis and glycosidase inhibition studies of novel triazole fused iminocyclitol- δ -lactams. *Organic & Biomolecular Chemistry*, 17(5), 1130–1140. <https://doi.org/10.1039/c8ob03084g>
- Shah, B., Modi, P., & Sagar, S. R. (2020). In silico studies on therapeutic agents for COVID-19: Drug repurposing approach. *Life Sciences*, 252(March), 117652. <https://doi.org/10.1016/j.lfs.2020.117652>
- Shang, J., Wan, Y., Luo, C., Ye, G., Geng, Q., Auerbach, A., & Li, F. (2020). Cell entry mechanisms of SARS-CoV-2. *Proceedings of the National Academy of Sciences*, 117(21), 11727–11734. <https://doi.org/10.1073/pnas.2003138117>
- Sureshkumar, B., Mary, Y. S., Panicker, C. Y., Suma, S., Armaković, S., Armaković, S. J., Van Alsenoy, C., & Narayana, B. (2020). Quinoline derivatives as possible lead compounds for anti-malarial drugs: Spectroscopic, DFT and MD study. *Arabian Journal of Chemistry*, 13(1), 632–648. <https://doi.org/10.1016/j.arabjc.2017.07.006>
- Vanqualef, E., Simon, S., Marquant, G., Garcia, E., Klimerak, G., Delepine, J. C., Cieplak, P., & Dupradeau, F.-Y. (2011). R.E.D. Server: A web service for deriving RESP and ESP charges and building force field libraries for new molecules and molecular fragments. *Nucleic Acids Res*, 39(Web Server issue), W511–W517. <https://doi.org/10.1093/nar/gkr288>
- Vatanserver, E. C., Yang, K., Kratch, K. C., Drelich, A., Cho, C.-C., Mellot, D. M., Xu, S., Tseng, C.-T K., & Liu, W. R. (2020). Targeting the SARS-CoV-2 main protease to repurpose drugs for COVID-19. bioRxiv: The preprint server for biology, <https://doi.org/10.1101/2020.05.23.112235>
- Yang, L., Skjevik, Å. A., Han Du, W. G., Noodleman, L., Walker, R. C., & Götz, A. W. (2016). Data for molecular dynamics simulations of B-type cytochrome c oxidase with the Amber force field. *Data in Brief*, 8, 1209–1214. <https://doi.org/10.1016/j.dib.2016.07.043>
- Yin, W., Mao, C., Luan, X., Shen, D.-D., Shen, Q., Su, H., Wang, X., Zhou, F., Zhao, W., Gao, M., Chang, S., Xie, Y.-C., Tian, G., Jiang, H.-W., Tao, S.-C., Shen, J., Jiang, Y., Jiang, H., Xu, Y., ... Xu, H. E. (2020). Structural basis for inhibition of the RNA-dependent RNA polymerase from SARS-CoV-2 by remdesivir. *Science (New York, N.Y.)*, 368(6498), 1499–1504. <https://doi.org/10.1126/science.abc1560>